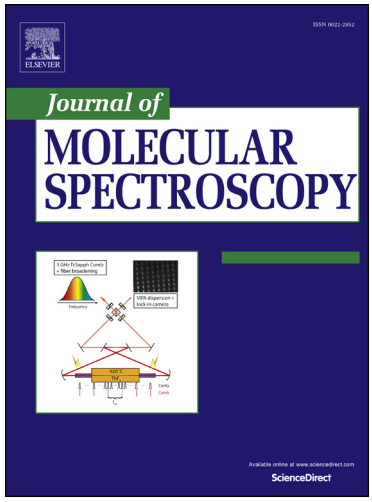

An *ab initio* study of SbH_2 and BiH_2: The Renner Effect, Spin-Orbit Coupling, Local Mode Vibrations and Rovibronic Energy Level Clustering in SbH_2

B. Ostojić, P. Schwerdtfeger, P.R. Bunker, Per Jensen

PII: S0022-2852(16)30033-9
DOI: http://dx.doi.org/10.1016/j.jms.2016.03.004
Reference: YJMSP 10690

To appear in: *Journal of Molecular Spectroscopy*

Received Date: 13 September 2015
Revised Date: 11 February 2016
Accepted Date: 9 March 2016

Please cite this article as: B. Ostojić, P. Schwerdtfeger, P.R. Bunker, P. Jensen, An *ab initio* study of SbH_2 and BiH_2: The Renner Effect, Spin-Orbit Coupling, Local Mode Vibrations and Rovibronic Energy Level Clustering in SbH_2, *Journal of Molecular Spectroscopy* (2016), doi: http://dx.doi.org/10.1016/j.jms.2016.03.004

An *ab initio* study of SbH_2 and BiH_2: The Renner Effect, Spin-Orbit Coupling, Local Mode Vibrations and Rovibronic Energy Level Clustering in SbH_2

B. Ostojić[a], P. Schwerdtfeger[b], P. R. Bunker[b,1], Per Jensen[c,*]

[a] *Institute of Chemistry, Technology and Metallurgy, University of Belgrade, Studentski trg 14-16, 11 000 Belgrade, Serbia*

[b] *Centre for Theoretical Chemistry and Physics (CTCP), The New Zealand Institute for Advanced Study(NZIAS), Massey University Auckland, Private Bag 102904, North Shore City, 0745 Auckland, New Zealand*

[c] *Physikalische und Theoretische Chemie, Fakultät für Mathematik und Naturwissenschaften, Bergische Universität, D-42097 Wuppertal, Germany*

Abstract

We present the results of *ab initio* calculations for the lower electronic states of the Group 15 (pnictogen) dihydrides, SbH_2 and BiH_2. For each of these molecules the two lowest electronic states become degenerate at linearity and are therefore subject to the Renner effect. Spin-orbit coupling is also strong in these two heavy-element containing molecules. For the lowest two electronic states of SbH_2, we construct the three dimensional potential energy surfaces and corresponding dipole moment and transition moment surfaces by multi-reference configuration interaction techniques. Including both the Renner effect and spin-orbit coupling, we calculate term values and simulate the rovibrational and rovibronic spectra of SbH_2. Excellent agreement is obtained with the results of matrix isolation infrared spectroscopic studies and with gas phase electronic spectroscopic studies in absorption. For the heavier dihydride BiH_2 we calculate bending potential curves and the spin-orbit coupling constant for comparison. For SbH_2 we further study the local mode vibrational behavior and the formation of rovibronic energy

*Corresponding author.

Email address: jensen@uni-wuppertal.de (Per Jensen)

URL: http://www.ptc.uni-wuppertal.de/jensen.html (Per Jensen)

[1] Permanent address: Steacie Laboratory, National Research Council of Canada, Ottawa, Ontario K1A0R6, Canada

level clusters in high angular momentum states.

Keywords: SbH_2, BiH_2, *ab initio* 3D potential energy surfaces, Renner effect, spin-orbit coupling, rovibrational spectra, local mode vibrations, rovibronic energy level clustering

1. INTRODUCTION

The Group 15 mono- (MH) and tri-hydrides (MH_3; M=N,...,Bi) are well studied both by spectroscopic and theoretical methods [1, 2, 3, 4, 5, 6, 7, 8]. The trihydrides all adopt a closed-shell $\boldsymbol{C}_{3v}$ structure with increasing inversion barrier toward the trigonal planar arrangement as the Group 15 element gets heavier, [9] while the monohydrides are all open-shell with a (spin-orbit split) $^3\Sigma^-$ ground state and a $^2\Pi$ excited state lying close by. [1] The lighter pnictogen dihydrides, NH_2 and PH_2, are the subject of many studies (see Refs. [10] and [11] and references therein), and the AsH_2 molecule is the subject of recent theoretical [12, 14] and experimental [15] work. However, there are no theoretical studies of the antimony and bismuth dihydrides at a level of precision appropriate for spectroscopic characterization. Here we fill this gap for SbH_2 and also perform connected *ab initio* calculations for BiH_2.

The two lowest lying electronic states of SbH_2 and BiH_2 are Renner-degenerate at linearity and subject to spin-orbit coupling. We focus mainly on SbH_2 in these two states, and to make useful spectroscopic predictions we determine the full three-dimensional potential energy surfaces of the two states, the dipole moment surfaces of the states, and the transition moment surface between the states; we also include spin-orbit coupling. With our computer program RENNER [10, 16, 17, 18], these surfaces are used to calculate rovibronic term values and to simulate the spectrum of SbH_2 in the infrared and visible spectral regions. The algorithm of our RENNER program involves using a Hund's case (a) basis set in which Λ and Σ are good quantum numbers, but it can be used satisfactorily for a case (c) molecule such as SbH_2. For BiH_2 we calculate the bending potentials for the lower-lying electronic states, and the spin-orbit coupling constant, for comparison.

The primary aim of the research is to see if our results are of help in confirming the identification of SbH_2 in three different experiments: The matrix isolation infrared spectrum obtained by reacting laser ablated Sb with hydrogen [19]; the visible absorption spectrum obtained by flash photolysis of stibine (SbH_3) [20]; and the visible emission spectrum obtained by UV laser

photolysis of stibine [21]. We also have some interest in determining the way the Renner effect and spin-orbit coupling change for the pnictogen dihydrides as one moves from the lightest (NH_2) to the heaviest (BiH_2). Having heavy central atoms and equilibrium bond angles close to 90°, these two XH_2 molecules are good candidates for exhibiting local mode vibrational behavior and for forming rovibronic energy level clusters; we study these aspects in quantitative detail for SbH_2. In addition to these purely spectroscopic concerns, the photophysics of antimony materials such as SbH_3 and SbH_2 is important for the understanding of the initiation and growth of antimonide materials during metalorganic chemical vapor deposition in the manufacture of semiconductor devices [22].

2. AB INITIO CALCULATIONS

The ground electronic and the first excited electronic states of SbH_2 and BiH_2 ($\boldsymbol{C}_{2v}$ point group) are of $\tilde{X}^2B_1$ and $\tilde{A}^2A_1$ symmetry respectively. These two states are components of the $1^2\Pi_u$ electronic state at linearity. We have computed energies on the potential energy surfaces of the $\tilde{X}^2B_1$ and $\tilde{A}^2A_1$ electronic states of SbH_2 and BiH_2 employing an all-electron complete active space self-consistent field (CASSCF) method [23, 24], followed by a multi-reference configuration interaction (MRCI) treatment [25, 26, 27]. For hydrogen we used a aug-cc-pV5Z basis set, [28] for antimony a Sapporo-DKH3-QZP-2012 basis set (extracted from the Sapporo Data Base of Segmented Gaussian Basis Sets [29]), and for bismuth a segmented all-electron contracted double zeta valence plus polarization function (DZP) basis set [30] constructed for use in conjunction with the non-relativistic and Douglas-Kroll-Hess (DKH) Hamiltonian [31, 32, 33]. We denote this basis set as DZP-DKH. The molecule is placed in the yz plane and in a linear geometry, z is taken as the molecular axis.

The most important configuration in the CASSCF calculation of the SbH_2 $\tilde{X}^2B_1$ electronic ground state is $|\ldots 12a_1{}^2\,6b_2{}^2\,13a_1{}^2\,6b_1{}^1\rangle$ (and for BiH_2 it is $|\ldots 18a_1{}^2\,10b_2{}^2\,19a_1{}^2\,10b_1{}^1\rangle$). For the SbH_2 $\tilde{A}^2A_1$ excited electronic state the most important configuration in the CASSCF procedure corresponds to the $13a_1 \rightarrow 6b_1$ excitation ($19a_1 \rightarrow 10b_1$ for BiH_2). At linearity the $6b_1$ and $13a_1$ highest occupied molecular orbitals (HOMOs) of SbH_2 correlate with the degenerate $4\pi_u$ MOs being composed mainly of Sb $5p_{x,y}$ orbitals perpendicular to the molecular axis. The SbH_2 $12a_1$ orbital consists mainly of a symmetric linear combination of H 1s orbitals combined with the Sb 5s

orbital. The $6b_2$ orbital is mainly an antisymmetric linear combination of H 1s orbitals combined with the Sb $5p_z$ orbital. A similar picture is obtained for BiH_2 (here the HOMO for the linear arrangement is the $7\pi_u$ orbital).

A full valence active space was employed in all the CASSCF calculations (three orbitals of a_1 symmetry, one of b_1, two of b_2, and none of a_2 symmetry). The active space consisted of all configurations obtained by distributing the 7 electrons ($1s^1$ on each H and $5s^25p^3$ on Sb for SbH_2 and $1s^1$ on each H and $6s^26p^3$ on Bi for BiH_2) in 6 MOs (12-14a_1, 6b_1, 6-7b_2 for SbH_2 and 18-20a_1, 10b_1, 10-11b_2 for BiH_2). For these two doublet electronic states ($\tilde{A}^2A_1$ and $\tilde{X}^2B_1$) we used a CASSCF state averaging (SA) procedure with equal weights. The CI expansion of the CASSCF wavefunction starting from the CAS(6,7) orbitals was generated within the internally contracted method using single and double substitutions (MRCISD) from each reference determinant. In these MRCISD calculations we have chosen to label the different molecular orbital spaces as follows: the core space contains nine orbitals of a_1 symmetry, four of b_1, four of b_2, and one of a_2 symmetry for SbH_2. The closed space contains two orbitals of a_1 symmetry, one of b_1, one of b_2, and one of a_2 symmetry which have predominantly 4d(Sb) character and were part of the closed space in the CASSCF calculations. In the MRCI calculations they were doubly occupied in all reference configuration state functions and correlated through single and double excitations. The active orbitals were 11 MOs (10-14a_1, 5-6b_1, 5-7b_2, 2a_2). In the MRCISD calculations of BiH_2 different molecular orbital spaces are labeled in the following manner: the core space contains fifteen orbitals of a_1 symmetry, eight of b_1, eight of b_2, and three of a_2 symmetry. The closed space contains two orbitals of a_1 symmetry, one of b_1, one of b_2, and one of a_2 symmetry which have predominantly 5d(Bi) character and were part of the closed space in the CASSCF calculations. In the MRCI calculations they were doubly occupied in all reference configuration state functions and correlated through single and double excitations. The active orbitals were 11 MOs (16-20a_1, 9-10b_1, 9-11b_2, 4a_2). The effect of higher excitations was taken into account by using the Davidson correction [28] (hereafter we denote this level of theory SA-CAS-MRCISD+Q and the corresponding energy as E_{MRCI}). Scalar relativistic effects were taken into account by applying the second-order Douglas–Kroll–Hess Hamiltonian (DKH) [31, 32, 33] as incorporated in the MOLPRO 2010.1 program package [34]. The two dipole moment surfaces for each electronic state of SbH_2 and transition moment surface between two electronic states of SbH_2 were obtained at the CAS-MRCISD level in the framework of the $\boldsymbol{C}_s$ point group.

Calculations of the potential and dipole moment surfaces for SbH_2 were made on a grid of 124 geometries with bond lengths from 1.45 to 2.05 Å and bond angles from 45° to 180°. We only calculate bending curves for the lower electronic states of BiH_2.

By interpolating our energies as a function of geometry we find that the $\tilde{X}$ ground electronic state of SbH_2 has an equilibrium bond length of 1.719 Å and an equilibrium bond angle of 90.5°. The optimum bond length at linearity was found to be 1.635 Å and the height of the barrier to linearity in ground state SbH_2 was obtained as 26582 cm^{-1}. The equilibrium geometry of $\tilde{A}$ state SbH_2 was determined as having a bond length of 1.681 Å and a bond angle of 121.3°; we obtained $T_e(\tilde{A}) = 19255$ cm^{-1}. In order to check the precision of our *ab initio* method we performed scalar relativistic Douglas-Kroll CCSD(T) calculations using augmented correlation consistent quadruple basis sets for Sb [35] and H [36]. The $\tilde{X}^2B_1$ equilibrium geometry has [r_e, $\angle_e$(H-Sb-H)] = [1.679 Å, 89.88°] whereas for the $\tilde{A}^2A_1$ state, the corresponding values are [1.643 Å, 120.67°]. Also, $T_e(\tilde{A}) = 19478$ cm^{-1}. The linear $^2\Pi_u$ is a saddle point connecting the two bent states, and has an optimum bond length of 1.589 Å. The height of the barrier to linearity for the $\tilde{X}^2B_1$ state is 26470 cm^{-1}. We note however that the linear $^2\Sigma_g^+$ state lies slightly below the $^2\Pi_u$ state by 1391 cm^{-1}, but has a much larger bond distance of 1.886 Å.

The ground electronic state of BiH_2 has an equilibrium Bi-H bond length of 1.803 Å and an equilibrium H-Bi-H angle of 89.7°; ground state BiH_2 has a barrier to linearity of 29464 cm^{-1}. We calculate the dipole moments of $\tilde{X}$-state SbH_2 and BiH_2 as 0.02 and 0.62 D, respectively, at the equilibrium geometries. The $\tilde{A}$←$\tilde{X}$ transition moments for SbH_2 and BiH_2, computed at the equilibrium geometry of the $\tilde{X}$ state, were found to be 1.11 and 1.46 D, respectively. Note that the larger dipole moment for BiH_2 compared to SbH_2 can easily be explained by looking at the trend down the group 15 dihydrides. From scalar relativistic MP2 calculations using double-zeta quality of basis sets we obtain (in D) NH_2 −2.32, PH_2 −1.14, AsH_2 −0.54, SbH_2 0.06, BiH_2 0.72 (Note: these dipole moments are only indicative to show the trend). This is can be understood from a decrease in electronegativity together with the increase in bond length and decrease in bond angle down the group 15 of elements, e.g. in the case of NH_2 we have the Mulliken charges of −0.48 for N and +0.24 for H, while for BiH_2 we have +0.12 for Bi and −0.06 for H.

Spin-orbit matrix elements were computed using the Breit-Pauli (BP) operator. The one and two electron BP terms in lowest order as imple-

mented in MOLPRO were used for computing the matrix elements between internal configurations of the MRCI wavefunctions (no electrons in external orbitals), while for contributions of external configurations a mean-free one-electron Fock operator is employed. The error caused by this approximation is considered to be negligible (smaller than 1 cm^{-1}). From this calculation a value of 3008 cm^{-1} was obtained for the spin-orbit coupling constant A_{SO} for the $1^2\Pi_u$ electronic state of SbH_2 at linearity with a bond length of 1.719 Å. For BiH_2 at linearity with a bond length of 1.803 Å, A_{SO} was calculated to be 11548 cm^{-1}. The value of the spin-orbit coupling constant at the equilibrium geometry (1.719 Å and 90.5°) for SbH_2 was calculated to be 2528 cm^{-1}. These are to be compared to the atomic spin-orbit coupling constants of 4384 and 13859 cm^{-1}, respectively, for the Sb^{2+} and Bi^{2+} ions [37].

3. THE POTENTIAL ENERGY AND DIPOLE MOMENT SURFACES

For these two molecules at linearity the ground electronic state is a $^2\Pi_u$ state, the first excited doublet electronic state is a $^2\Sigma_g^-$ state, and the second excited doublet electronic state is a $^2\Delta_g$ state. At bent configurations the $^2\Pi_u$ state splits into the lower $\tilde{X}^2B_1$ state and the upper $\tilde{A}^2A_1$ state, the $^2\Sigma_g^-$ state correlates with the 2^2B_1 state, and the $^2\Delta_g$ state splits into the lower 2^2A_1 state and the upper 3^2B_1 state. At small bond angles there is an avoided crossing between the $\tilde{A}^2A_1$ state and the 2^2A_1 state. This is all exactly as for AsH_2 (see Fig. 1 of Ref. [12]). For the SbH_2 molecule we have determined the bending potential curves of these five states when the Sb-H bond length is held fixed at 1.719 Å, and these are shown in Fig. 1. For the BiH_2 molecule we have determined the bending potential curves of these five states when the Bi-H bond length is held fixed at 1.803 Å, and these are shown in Fig. 2. For the rest of this paper we consider only the $\tilde{X}$ and $\tilde{A}$ states of SbH_2 and in this section we focus on the problem of parameterizing the potential energy, dipole moment and transition moment surfaces for these two electronic states. The computations of the *ab initio* points displayed in Figs. 1 and 2 involve the six electronic states labeled in the figures. Consequently, the computed values of the $\tilde{X}$- and $\tilde{A}$-state electronic energies of SbH_2 displayed in Fig. 1 differ marginally from those used as input for the fitting of the analytical potential energy functions (detailed below and displayed in Fig. 3) which included only the two states $\tilde{X}$ and $\tilde{A}$.

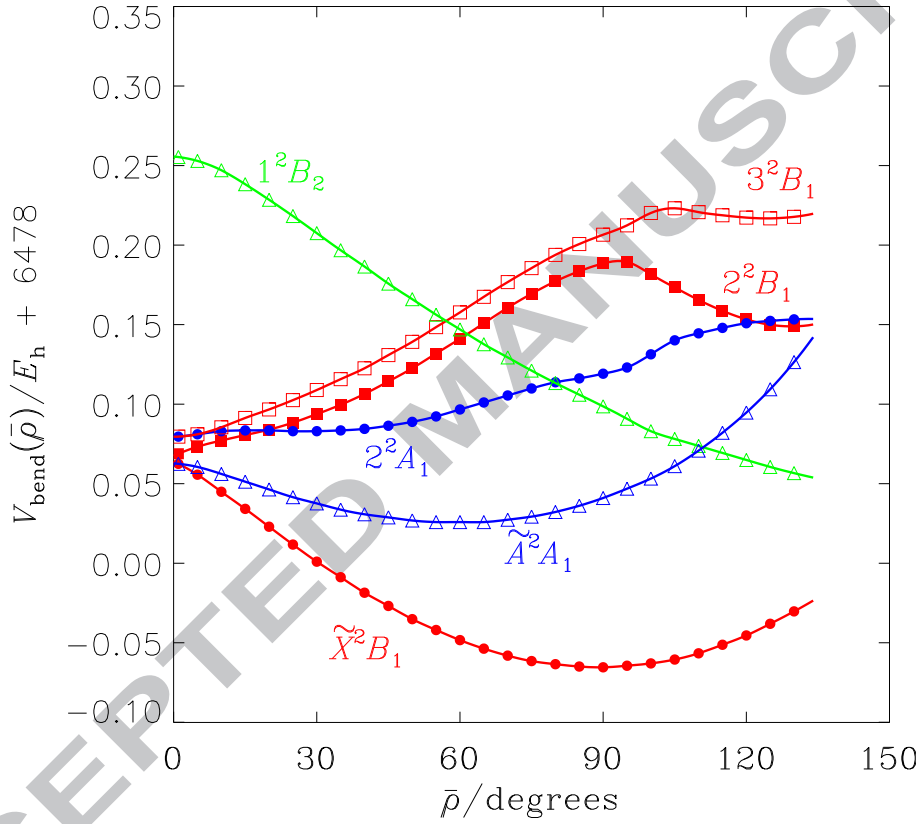

Figure 1: Bending potential energy curves for the six lowest electronic states of SbH_2, obtained with the Sb–H bond lengths held fixed at 1.719 Å. The energies are plotted against $\bar{\rho} = 180° - \angle$(HSbH).

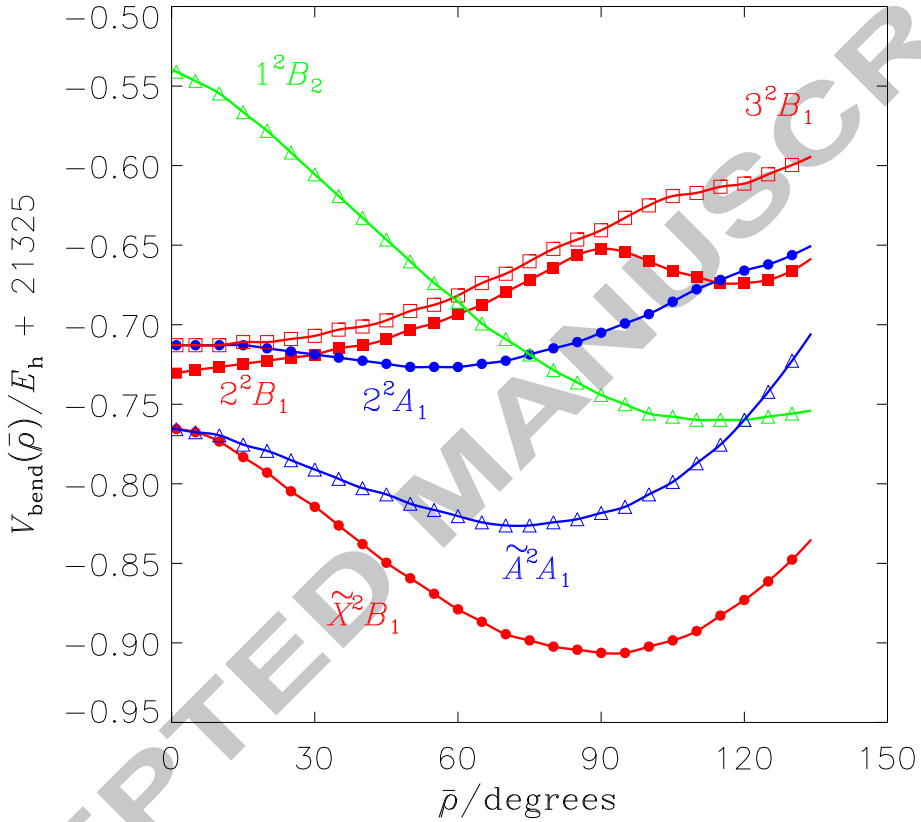

Figure 2: Bending potential energy curves for the six lowest electronic states of BiH_2, obtained with the Bi–H bond lengths held fixed at 1.803 Å. The energies are plotted against $\bar{\rho} = 180° - \angle(\mathrm{HBiH})$.

In the RENNER program (see, for example, Ref. [16]), the lower and upper potential energy surfaces of a Renner pair, $V_-(\Delta r_{12}, \Delta r_{32}, \bar{\rho})$ and $V_+(\Delta r_{12}, \Delta r_{32}, \bar{\rho})$ respectively, are written

$$V_\pm(\Delta r_{12}, \Delta r_{32}, \bar{\rho}) = V_0^{(\pm)}(\bar{\rho}) + \sum_j F_j^{(\pm)}(\bar{\rho}) y_j + \sum_{j \le k} F_{jk}^{(\pm)}(\bar{\rho}) y_j y_k + \sum_{j \le k \le m} F_{jkm}^{(\pm)}(\bar{\rho}) y_j y_k y_m + \sum_{j \le k \le m \le n} F_{jkmn}^{(\pm)}(\bar{\rho}) y_j y_k y_m y_n, \quad (1)$$

with

$$y_j = 1 - \exp(-a_1 \Delta r_{j2}), \quad (2)$$

$$F_{jk\ldots}^{(\pm)}(\bar{\rho}) = f_{jk\ldots}^{(0)} + \sum_{i=1}^{N} f_{jk\ldots}^{(i,\pm)} (1 - \cos\bar{\rho})^i, \quad (3)$$

and

$$V_0^{(\pm)}(\bar{\rho}) = \sum_{i=1}^{8} f_0^{(i,\pm)} (1 - \cos\bar{\rho})^i. \quad (4)$$

In Eq. (1), $\bar{\rho}$ is the instantaneous value of the bond angle supplement (see Fig. 15-14 of Ref. [38]), and $\Delta r_{j2} = r_{j2} - r^{(\mathrm{ref})}$, where the r_{j2} are the instantaneous Sb-H$_j$ bond lengths and $r^{(\mathrm{ref})}$ is the reference value of these quantities, which is taken here as the equilibrium bond length of the ground state, $r^{(\mathrm{ref})}$ = 1.719 Å, as determined by interpolating the *ab initio* energies; the indices j, k, m, and n can each be 1 or 3. In Eq. (2), a_1 is a molecular parameter. In Eq. (3), the parameters $f_{jk\ldots}^{(0)}$ are common for the two potential energy surfaces and this ensures that the functions are degenerate at linearity when $\bar{\rho} = 0$; the function $F_j^{(\pm)}(\bar{\rho})$ has $N = 4$, $F_{jk}^{(\pm)}(\bar{\rho})$ has $N = 3$, $F_{jkl}^{(\pm)}(\bar{\rho})$ has $N = 2$, and $F_{jklm}^{(\pm)}(\bar{\rho})$ has $N = 1$. The adjustable parameters $f_{\ldots}^{()}$ in V_- and V_+ are constrained to ensure that V_- and V_+ are totally symmetric under the interchange of Δr_{12} and Δr_{32} which they must be for a symmetrical molecule like SbH_2.

We usually determine the values of the parameters in Eqs. (1-4) in a simultaneous least squares fitting to the *ab initio* energies for both electronic states involved. For SbH_2, however, we encountered difficulties in the initial fitting caused by the fact that at small bond angles the $\tilde{A}$-state potential suffers an avoided crossing with that of the 2^2A_1 state (see Fig. 1). In order to obtain an approximate diabatic potential energy function for the $\tilde{A}$ state (i.e., an approximation of the potential energy function that $\tilde{A}^2A_1$ SbH_2

would have had in the absence of the avoided crossing), we initially made a separate fitting of the $\tilde{X}$-state *ab initio* energies to the so-called MORBID expansion [13] in the quantities $y_{\rm b}^{\rm (M)} = \cos\rho_{\rm e} - \cos\bar{\rho}$, where $\rho_{\rm e}$ is the equilibrium value of $\bar{\rho}$ in the $\tilde{X}$ state, and

$$y_j^{\rm (M)} = 1 - \exp[-a_1(r_{j2} - r^{\rm (e)})], \quad j = 1 \ \text{ or } \ 3. \tag{5}$$

In general, $y_j^{\rm (M)}$ will differ from y_j in Eq. (2) because the reference bond length $r^{\rm (ref)}$ can, and often will, be chosen to be different from $r^{\rm (e)}$, the equilibrium bond length value for the electronic state considered. In the particular case of $\tilde{X}$-state SbH_2 considered here, we have chosen $r^{\rm (ref)} = r^{\rm (e)}$ and so $y_j^{\rm (M)} = y_j$. In the initial fitting, the input data set comprised 110 $\tilde{X}$-state data points and we obtained a standard deviation of 46.1 $\rm cm^{-1}$. This value is somewhat larger than those we typically obtain in this type of fitting but the energy range covered by the *ab initio* points exceeds 30000 $\rm cm^{-1}$ here, and so this range is considerably larger than those we typically consider. This limits the achievable quality of the fitting.

The parameterized function in Eqs. (1-4) is an expansion in the quantities $y_{\rm b}^{\rm (R)} = 1 - \cos\bar{\rho}$, $y_1 = y_1^{\rm (M)}$, and $y_3 = y_3^{\rm (M)}$. Owing to the identity $y_{\rm b}^{\rm (M)} = \cos\rho_{\rm e} - 1 + y_{\rm b}^{\rm (R)}$ we can convert exactly the fitted analytical representation of the $\tilde{X}$-state potential energy function to the form of Eqs. (1)-(4).

For the $\tilde{A}^2A_1$ state, we make a separate fit of the *ab initio* points (having given low weights to a number of points near the avoided crossing) to the MORBID expansion in $y_{\rm b}^{\rm (M)}$, $y_1^{\rm (M)}$, and $y_3^{\rm (M)}$, obtaining a fitting to 107 data points with a standard deviation of 51.8 $\rm cm^{-1}$. This untypically large value is primarily caused by 'outliers' near the avoided crossing and at higher energies, in particular at and near the linear geometries, i.e., at the top of the barrier to linearity. The residuals for points near the $\tilde{A}$-state minimum are generally a few $\rm cm^{-1}$. It is not viable to remove the outlier points from the fittings since this leads to fitted potentials with spurious minima or 'holes'. The initial $\tilde{A}$-state fitting produced values of $r^{\rm (e)} = 1.66511(75)$ Å and $\rho_{\rm e} = 59.11(25)^\circ$ for this state (where one standard error in units of the least significant digit is given in parentheses), and since the value of $r^{\rm (ref)} = 1.719$ Å is common for the two electronic states, we now have $r^{\rm (ref)} \neq r^{\rm (e)}$. In this case, we employ the general identity

$$y_j^{\rm (M)} = 1 - \exp[a_1\left(r^{\rm (e)} - r^{\rm (ref)}\right)]\,(1 - y_j)\,, \quad j = 1 \ \text{ or } \ 3, \tag{6}$$

together with $y_{\rm b}^{\rm (M)} = \cos\rho_{\rm e} - 1 + y_{\rm b}^{\rm (R)}$, to convert the $\tilde{A}$-state potential energy function to the form of Eqs. (1)-(4). We take the parameters $f_{jk...}^{(0)}$ in Eq. (3), which are common to the two electronic states, as the values obtained for the $\tilde{X}$ state. The resulting set of potential energy parameter values for the $\tilde{X}$ and $\tilde{A}$ states is given in Table 1. We use these parameters, with the spin-orbit coupling parameter $A_{\rm SO} = 2528$ cm^{-1} in the RENNER program to calculate rovibronic energies and wavefunctions.

The RENNER calculations yield, for a level with a given value of the rotational angular momentum quantum number N, the F_1 fine structure component with $J = N+\frac{1}{2}$ and the F_2 component with $J = N-\frac{1}{2}$ and are carried out with the following basis sets, chosen after having made convergence tests for the high angular momentum states involved:

(a) For the $\tilde{X}$ and $\tilde{A}$ states, we use $N_{\rm Bend} = 15$ lowest bending basis functions. The stretching function basis was selected using Morse oscillator functions $|n_1 n_3\rangle$ having $n_1 + n_3 \leq N_{\rm Stretch} = 12$ for both electronic states. Of these functions we used the $N_A = 12$ lowest stretching basis functions of A_1 symmetry, and the $N_B = 6$ lowest stretching basis functions of B_2 symmetry, again for both electronic states. The contraction step [18] was made with a cut-off energy of $E_{\rm limit} = 35000$ cm^{-1}.

(b) $N_{\rm Bend} = 15(10)$ for the $\tilde{X}(\tilde{A})$ electronic state state together with $N_{\rm Stretch} = 13$ and $(N_A, N_B) = (12,6)$ for both electronic states. $E_{\rm limit} = 35000$ cm^{-1}.

(c) $N_{\rm Bend} = 8$, $N_{\rm Stretch} = 7$, and $(N_A, N_B) = (6,4)$ for both electronic states. $E_{\rm limit} = 35000$ cm^{-1}.

(d) $N_{\rm Bend} = 8$, $N_{\rm Stretch} = 7$, and $(N_A, N_B) = (6,4)$ for both electronic states. $E_{\rm limit} = 50000$ cm^{-1}.

With basis set (a), we calculate rovibronic energies of $^{121}SbH_2$, $^{121}SbD_2$, and $^{121}SbHD$ for $J \leq 19/2$. With basis set (b), we simulate absorption spectra for the $\tilde{X}$ and $\tilde{A}$ states of $^{121}SbH_2$ and $^{123}SbH_2$. With basis set (c) we simulate emission spectra of $^{121}SbH_2$ and $^{123}SbH_2$ for $J \leq 49/2$ (see Section 4 below) and finally, with basis set (d) we calculate rovibronic energies for $J \leq 79/2$ in order to investigate the formation of rovibronic energy clusters in $^{121}SbH_2$ (see Section 5 below).

From the determinations of analytic expressions for the potential surfaces of the $\tilde{X}$ and $\tilde{A}$ states of SbH_2, and the calculations of the rovibronic energies

Table 1: The nonzero potential energy parameters (in cm^{-1} unless otherwise indicated) for the $\widetilde{X}\,^2B_1$ and $\widetilde{A}\,^2A_1$ states of SbH_2 [see Eqs. (1)–(4)].

$r^{(\mathrm{ref})}$/Å	1.719	
a_1/Å^{-1}	1.408	
$f_1^{(0)}$	−1915.1	
$f_{11}^{(0)}$	18068.2	
$f_{13}^{(0)}$	−1954.0	
$f_{111}^{(0)}$	−11171.7	
$f_{113}^{(0)}$	6396.9	
$f_{1111}^{(0)}$	−1965.8	
	$\widetilde{X}\,^2B_1(\sigma=-)$	$\widetilde{A}\,^2A_1(\sigma=+)$
$f_0^{(1,\sigma)}$	−168532.0	−80528.8
$f_0^{(2,\sigma)}$	734266.0	409860.2
$f_0^{(3,\sigma)}$	−2132075.1	−1334990.4
$f_0^{(4,\sigma)}$	3745904.9	2702040.3
$f_0^{(5,\sigma)}$	−3939015.2	−3286462.0
$f_0^{(6,\sigma)}$	2424677.6	2326513.0
$f_0^{(7,\sigma)}$	−803630.9	−876210.7
$f_0^{(8,\sigma)}$	110555.0	134878.0
$f_1^{(1,\sigma)}$	12769.1	−5549.5
$f_1^{(2,\sigma)}$	−19338.3	33300.4
$f_1^{(3,\sigma)}$	14284.3	−44695.0
$f_1^{(4,\sigma)}$	−4457.0	20450.9
$f_{11}^{(1,\sigma)}$	31721.5	17571.1
$f_{11}^{(2,\sigma)}$	−37042.6	12372.7
$f_{11}^{(3,\sigma)}$	13497.2	−6851.8
$f_{13}^{(1,\sigma)}$	−2090.5	−8556.5
$f_{13}^{(2,\sigma)}$	6206.4	4931.1
$f_{13}^{(3,\sigma)}$	−2097.2	1261.7
$f_{111}^{(1,\sigma)}$	29056.5	−7097.7
$f_{111}^{(2,\sigma)}$	−17612.9	
$f_{113}^{(1,\sigma)}$	−17252.9	568.9
$f_{113}^{(2,\sigma)}$	10207.6	
$f_{1111}^{(1,\sigma)}$	8198.3	−8048.5
$f_{1113}^{(1,\sigma)}$		1705.2
$f_{1133}^{(1,\sigma)}$		3567.9

associated with them, we can draw Fig. 3. This figure shows the bending potential energy curves of SbH_2, in the $\tilde{X}$ and $\tilde{A}$ states, with the bond lengths held fixed at 1.719 Å, and the energies of the lowest bending eigenstates having $K_a = 0$. As detailed above, the fitted potential energy surfaces are obtained by first carrying out separate fits of the $\tilde{X}$- and $\tilde{A}$-state points and subsequently forcing the two fitted functions to be degenerate at linearity.

To calculate intensities we use analytical functions for the dipole moment and transition moment surfaces, as first explained in Ref. [18]. And, as with the potential surface parameters we determine the dipole and transition moment parameters in a least squares fitting to the *ab initio* values. In the *ab initio* calculation of the dipole moments and transition moment we define three axes xqp, with origin in the nuclear center of mass, which are attached directly to the instantaneous nuclear configuration of the molecule (see Fig. 1 of Ref. [39]). For SbH_2 at any nuclear configuration, the q axis is defined as bisecting the bond angle $\angle$(HSbH) and is directed so that the q coordinates of the H nuclei 1 and 3 are positive. The p axis is perpendicular to the q axis in the HSbH plane and its direction is such that the p coordinate of nucleus 3 is positive. The x axis is perpendicular to the molecular plane and directed so that xqp is right-handed.

We denote the electronic wavefunction for the $\widetilde{X}$ state as $\psi^{(-)}_{\rm elec}$ and that for the $\widetilde{A}$ state as $\psi^{(+)}_{\rm elec}$. In this notation we obtain the following non-vanishing dipole and transition moments:

$$\bar{\mu}^{(\sigma)}_p(\Delta r_{12}, \Delta r_{32}, \bar{\rho}) = \langle \psi^{(\sigma)}_{\rm elec} | \mu_p | \psi^{(\sigma)}_{\rm elec} \rangle_{\rm el}, \tag{7}$$

$$\bar{\mu}^{(\sigma)}_q(\Delta r_{12}, \Delta r_{32}, \bar{\rho}) = \langle \psi^{(\sigma)}_{\rm elec} | \mu_q | \psi^{(\sigma)}_{\rm elec} \rangle_{\rm el} \tag{8}$$

where, in Eqs. (7) and (8), $\sigma = -$ or $+$, and

$$\bar{\mu}^{(-+)}_x(\Delta r_{12}, \Delta r_{32}, \bar{\rho}) = \langle \psi^{(-)}_{\rm elec} | \mu_x | \psi^{(+)}_{\rm elec} \rangle_{\rm el}. \tag{9}$$

where, in Eqs. (7)-(9), the subscript 'el' indicates that integration is over the electronic coordinates only.

The functions $\bar{\mu}^{(\sigma)}_p$ and $\bar{\mu}^{(\sigma)}_q$ are represented as (see Ref. [39])

$$\begin{aligned} \bar{\mu}^{(\sigma)}_p(\Delta r_{12}, \Delta r_{32}, \bar{\rho}) &= \mu^{(p;\sigma)}_0(\bar{\rho}) \\ &+ \sum_j \mu^{(p;\sigma)}_j(\bar{\rho}) \Delta r_{j2} + \sum_{j \le k} \mu^{(p;\sigma)}_{jk}(\bar{\rho}) \Delta r_{j2} \Delta r_{k2} \end{aligned}$$

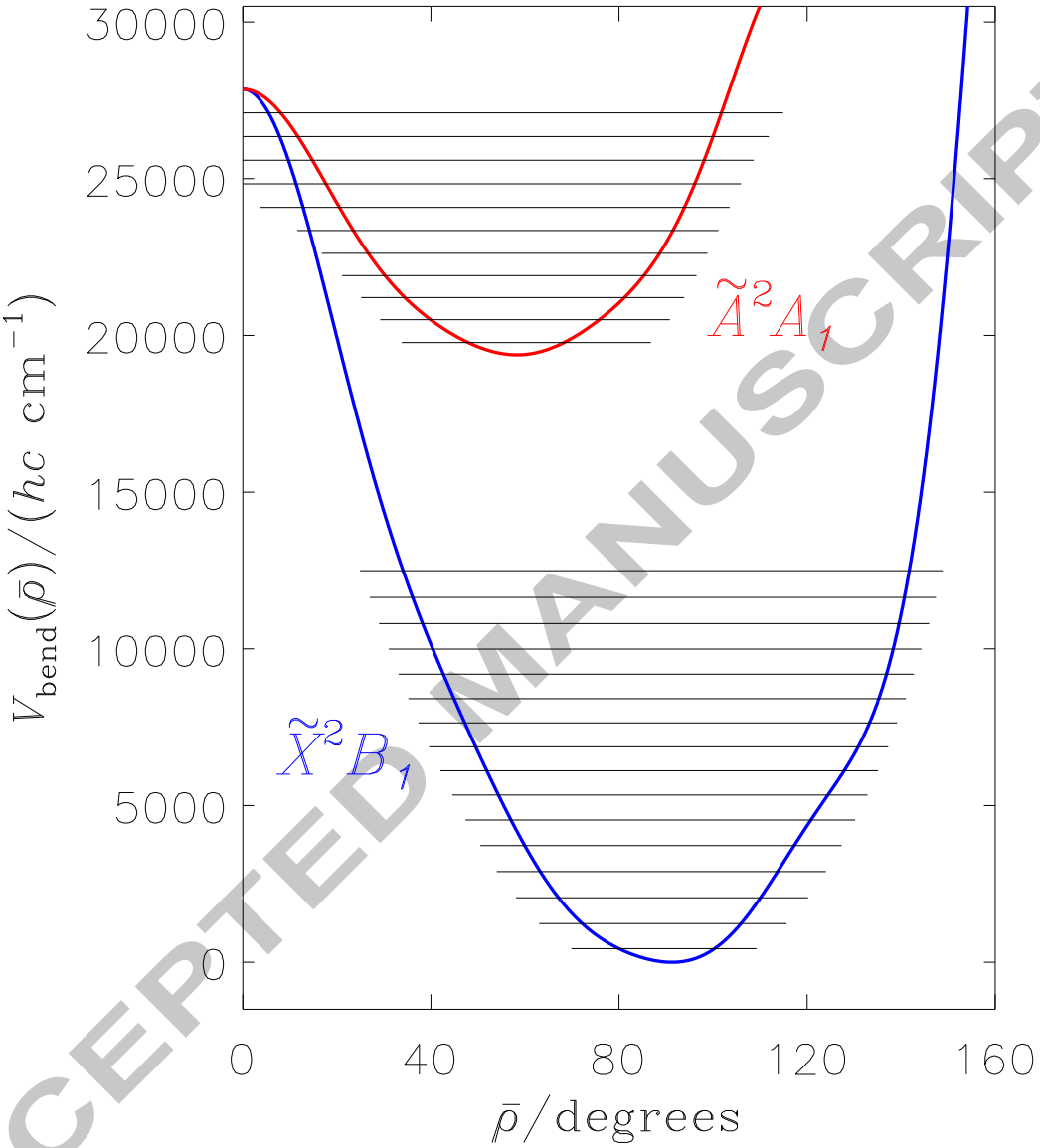

Figure 3: The bending potential energy functions of SbH_2 in the $\tilde{X}^2B_1$ and $\tilde{A}^2A_1$ electronic states. The electronic energies are plotted against $\bar{\rho} = 180° - \angle(\mathrm{HSbH})$; the bond lengths are both held fixed at the value $r^{(\mathrm{ref})} = 1.719$ Å. The energies of the 16(11) lowest bending eigenstates with $K_a = 0$ and $v_2 = 0, 1, 2, \ldots, 15(10)$ are indicated for the $\tilde{X}(\tilde{A})$ state. In the text we explain how these two potentials were obtained by fitting to the *ab initio* points.

$$+ \sum_{j\le k\le m} \mu_{jkm}^{(p;\sigma)}(\bar{\rho})\Delta r_{j2}\Delta r_{k2}\Delta r_{m2}$$
$$+ \sum_{j\le k\le m\le n} \mu_{jkmn}^{(p;\sigma)}(\bar{\rho})\Delta r_{j2}\Delta r_{k2}\Delta r_{m2}\Delta r_{n2} \quad (10)$$

and

$$\bar{\mu}_q^{(\sigma)}(\Delta r_{12},\Delta r_{32},\bar{\rho}) = \sin\bar{\rho}\Big[\mu_0^{(q;\sigma)}(\bar{\rho})$$
$$+ \sum_j \mu_j^{(q;\sigma)}(\bar{\rho})\Delta r_{j2} + \sum_{j\le k} \mu_{jk}^{(q;\sigma)}(\bar{\rho})\Delta r_{j2}\Delta r_{k2}$$
$$+ \sum_{j\le k\le m} \mu_{jkm}^{(q;\sigma)}(\bar{\rho})\Delta r_{j2}\Delta r_{k2}\Delta r_{m2}$$
$$+ \sum_{j\le k\le m\le n} \mu_{jkmn}^{(q;\sigma)}(\bar{\rho})\Delta r_{j2}\Delta r_{k2}\Delta r_{m2}\Delta r_{n2}\Big], \quad (11)$$

with j, k, m, $n = 1$ or 3. The angle-dependent coefficients are given by

$$\mu_{jk\ldots}^{(w;\sigma)}(\bar{\rho}) = \sum_{i=0}^{N} w_{jk\ldots}^{(i;\sigma)}(1-\cos\bar{\rho})^i, \quad (12)$$

with w= p or q. The function $\mu_0^{(w;\sigma)}(\bar{\rho})$ has $N = 8$, $\mu_j^{(w;\sigma)}(\bar{\rho})$ has $N = 4$, $\mu_{jk}^{(w;\sigma)}(\bar{\rho})$ has $N = 3$, $\mu_{jkm}^{(w;\sigma)}(\bar{\rho})$ has $N = 2$ and $\mu_{jkmn}^{(w;\sigma)}(\bar{\rho})$ has $N = 1$.

The function $\bar{\mu}_x^{(-+)}$ is parameterized as

$$\bar{\mu}_x^{(-+)}(\Delta r_{12},\Delta r_{32},\bar{\rho}) = \sin\bar{\rho}\Big[\mu_0^{(x;-+)}(\bar{\rho})$$
$$+ \sum_j \mu_j^{(x;-+)}(\bar{\rho})\Delta r_{j2} + \sum_{j\le k} \mu_{jk}^{(x;-+)}(\bar{\rho})\Delta r_{j2}\Delta r_{k2}$$
$$+ \sum_{j\le k\le m} \mu_{jkm}^{(x;-+)}(\bar{\rho})\Delta r_{j2}\Delta r_{k2}\Delta r_{m2}$$
$$+ \sum_{j\le k\le m\le n} \mu_{jkmn}^{(x;-+)}(\bar{\rho})\Delta r_{j2}\Delta r_{k2}\Delta r_{m2}\Delta r_{n2}\Big], \quad (13)$$

with

$$\mu_{jk\ldots}^{(x;-+)}(\bar{\rho}) = \sum_{i=0}^{N} x_{jk\ldots}^{(i;-+)}(1-\cos\bar{\rho})^i, \quad (14)$$

where the number of summation terms N is given exactly as for Eq. (12).

For a symmetrical molecule like SbH_2, relations exist between the expansion coefficients in Eqs. (12) and (14), so that the functions $\bar{\mu}_q^{(\sigma)}$ and $\bar{\mu}_x^{(-+)}$ are unchanged under the interchange of the two protons, whereas the function $\bar{\mu}_p^{(\sigma)}$ is antisymmetric under this operation.

For the dipole moment and transition moment surfaces we obtain values for the $p_{jk...}^{(i;\sigma)}$, $q_{jk...}^{(i;\sigma)}$, and $x_{jk...}^{(i;-+)}$ parameters by fitting Eqs. (10)-(14) through the *ab initio* dipole moment and transition moment values. The results of the fittings (parameter values, standard errors and the standard deviations of the fittings) are given in Table 2.

4. TERM VALUES AND SIMULATED SPECTRA FOR SbH_2

With the RENNER basis set (a) described above, we have calculated rovibronic term values of $\tilde{X}^2B_1$ and $\tilde{A}^2A_1$ $^{121}SbH_2$, $^{121}SbD_2$ and $^{121}SbHD$ for $J \leq 19/2$. The resulting term values with $N = 0$ and 1 are given in Tables 3–6. We have used basis set (b) (with $J \leq 19/2$) for simulations of the absorption spectrum of $^{121}SbH_2$ in the wavenumber region below 24000 cm^{-1}. However, the only transitions of appreciable intensity found in this spectrum are $\tilde{X}$-state transitions starting in the vibrational ground state and the $\tilde{A} \leftarrow \tilde{X}$ electronic spectrum, where the $\tilde{A} \leftarrow \tilde{X}$ transitions are much stronger than those in the $\tilde{X}$-state spectrum as shown by Figs. 4 and 5. The spectra in these figures are obtained for $^{121}SbH_2$ and $^{123}SbH_2$ in their natural abundances of 57.36% and 42.64%, respectively. As mentioned above, $\tilde{X}^2B_1$ SbH_2 has a very small permanent dipole moment of only 0.02 D, and so the rotational spectrum is too weak to be seen in Fig. 4.

In the matrix isolation infrared spectroscopic work of Ref. [19], laser ablated Sb atoms were reacted with hydrogen during condensation in six different environments: pure H_2, Ne/H_2, Ar/H_2, pure D_2, Ne/D_2, Ar/D_2, and Ar/HD. In each environment, two bands were identified as the $\tilde{X}$-state stretching vibrational fundamentals of SbH_2, SbD_2, or SbHD. In Table 7, we have summarized the experimental results and compared them to our predicted fundamental wavenumbers. The comparison obviously supports the assignment to SbH_2, SbD_2, and SbHD, respectively. However, our calculations predict that for SbH_2 and SbD_2, $E(\nu_1) > E(\nu_3)$ whereas the assignment of Ref. [19] assumes the more usual situation of $E(\nu_3) > E(\nu_1)$ as is encountered, for example, for NH_2 [10]. We discuss this further in Section 6.

Table 2: The *ab initio* dipole and transition moment parameters for the $\widetilde{X}$ and $\widetilde{A}$ electronic states of SbH_2 (see Eqs. (10)–(14)).

	$\widetilde{X}\ ^2B_1$		$\widetilde{A}\ ^2A_1$
$q_0^{(0;-)}$/D	7.828	$q_0^{(0;+)}$/D	0.889
$q_1^{(0;-)}$/D Å^{-1}	−5.168	$q_1^{(0;+)}$/D Å^{-1}	−1.407
$q_{111}^{(0;-)}$/D Å^{-3}	3.739	$q_1^{(1;+)}$/D Å^{-1}	1.657
$q_0^{(1;-)}$/D	−20.181	$q_0^{(2;+)}$/D	−5.930
$q_1^{(1;-)}$/D Å^{-1}	1.316	$q_0^{(3;+)}$/D	4.210
$q_0^{(2;-)}$/D	21.780	St.Dev.[a]/D	0.082
$q_0^{(3;-)}$/D	−11.819		
$q_0^{(4;-)}$/D	2.336		
St.Dev.[a]/D	0.040		
$p_1^{(0;-)}$/D Å^{-1}	2.953	$p_1^{(1;+)}$/D Å^{-1}	1.599
$p_1^{(1;-)}$/D Å^{-1}	1.755	$p_1^{(2;+)}$/D Å^{-1}	−0.930
$p_1^{(2;-)}$/D Å^{-1}	−0.845	$p_{11}^{(0;+)}$/D Å^{-2}	1.056
$p_{11}^{(0;-)}$/D Å^{-2}	1.050	$p_{11}^{(1;+)}$/D Å^{-2}	−5.234
$p_{11}^{(0;-)}$/D Å^{-2}	−1.106	St.Dev.[a]/D	0.073
$p_{111}^{(0;-)}$/D Å^{-3}	−2.517		
St.Dev.[a]/D	0.004		
	$\widetilde{X}/\widetilde{A}$		
$x_0^{(0;-+)}$/D	4.564	$x_1^{(1;-+)}$/D Å^{-1}	−0.383
$x_1^{(0;-+)}$/D Å^{-1}	−0.880	$x_0^{(2;-+)}$/D	4.463
$x_{11}^{(0;-+)}$/D Å^{-2}	−0.905	$x_0^{(3;-+)}$/D	−1.051
$x_0^{(1;-+)}$/D	−5.161	St.Dev.[a]/D	0.025

[a]Standard deviation of the fitting to the *ab initio* points.

Table 3: Calculated rovibronic term values (in cm^{-1}) for selected (v_1, v_2, v_3) states of $\tilde{X}^2B_1$ $^{121}SbH_2$.

$N_{K_aK_c}$	0_{00}	1_{01}		1_{11}		1_{10}	
(v_1, v_2, v_3)	F_1[a]	F_2[a]	F_1[a]	F_2	F_1	F_2	F_1
(0,0,0)	0.000	8.582	8.656	7.442	9.318	10.330	12.174
(0,1,0)	805.280	813.809	813.885	812.861	814.915	815.757	817.763
(0,2,0)	1628.326	1636.911	1636.987	1635.792	1637.979	1638.809	1640.933
(0,0,1)	1873.416	1881.916	1881.985	1880.784	1882.579	1883.657	1885.427
(1,0,0)	1876.016	1884.482	1884.558	1883.397	1885.221	1886.241	1888.034
(0,3,0)	2461.525	2470.214	2470.288	2468.170	2470.479	2471.358	2473.587
(1,1,0)	2675.052	2683.314	2683.509	2682.518	2684.531	2685.361	2687.320
(0,1,1)	2676.013	2684.449	2684.513	2683.687	2685.542	2686.404	2688.338
(0,4,0)	3292.532	3301.383	3301.449	3297.996	3300.430	3301.404	3303.734
(1,2,0)	3493.939	3502.316	3502.439	3500.977	3503.116	3503.927	3506.009
(0,2,1)	3495.061	3503.541	3503.616	3503.137	3505.201	3506.017	3508.071
(1,0,1)	3702.653	3711.095	3711.067	3710.732	3712.544	3713.574	3715.297
(0,0,2)	3703.407	3711.807	3711.814	3710.549	3712.400	3713.442	3715.169
(2,0,0)	3749.703	3758.072	3758.137	3756.820	3758.573	3759.631	3761.354
(0,5,0)	4105.994	4115.114	4115.174	4112.392	4114.959	4116.113	4118.548
(1,3,0)	4321.482	4330.008	4330.088	4328.238	4330.470	4331.365	4333.554
(0,3,1)	4322.372	4330.973	4331.077	4332.742	4334.969	4335.832	4337.991
(1,1,1)	4498.581	4507.035	4506.930	4508.990	4510.911	4511.750	4513.639
(0,1,2)	4499.377	4507.648	4507.728	4506.707	4508.820	4509.657	4511.554
(2,1,0)	4551.161	4559.465	4559.525	4557.679	4559.611	4560.469	4562.354
(0,6,0)	4888.896	4898.347	4898.407	4896.833	4899.538	4900.950	4903.494
(1,4,0)	5138.520	5147.196	5147.285	5145.736	5148.229	5149.125	5151.417
(0,4,1)	5138.564	5147.366	5147.333	5149.832	5152.169	5153.178	5155.438
(1,2,1)	5309.909	5318.288	5318.294	5321.756	5323.824	5324.651	5326.657
(0,2,2)	5310.437	5318.772	5318.835	5317.552	5319.689	5320.496	5322.515
(2,2,0)	5366.482	5374.845	5374.899	5373.003	5375.069	5375.913	5377.914
(1,0,2)	5488.570	5496.807	5496.865	5496.094	5497.801	5498.877	5500.546
(0,0,3)	5498.515	5506.768	5506.810	5507.157	5508.847	5509.919	5511.574
(2,0,1)	5586.152	5594.445	5594.474	5593.229	5595.066	5596.054	5597.688
(3,0,0)	5586.375	5594.627	5594.508	5593.096	5594.813	5595.839	5597.505
(0,7,0)	5648.348	5658.131	5658.190	5655.396	5658.269	5659.897	5662.572
(0,5,1)	5936.703	5945.837	5945.730	5943.718	5946.113	5947.476	5949.856
(1,5,0)	5938.417	5947.446	5947.619	5945.164	5947.872	5948.948	5951.354

[a]An F_2 state has $J = N - 1/2$; an F_1 state has $J = N + 1/2$.

Table 4: Calculated rovibronic term values (in cm^{-1}) for selected (v_1, v_2, v_3) states of $\tilde{X}^2B_1$ $^{121}SbD_2$.

$N_{K_aK_c}$	0_{00}	1_{01}		1_{11}		1_{10}	
(v_1, v_2, v_3)	F_1[a]	F_2[a]	F_1[a]	F_2	F_1	F_2	F_1
(0,0,0)	0.000	4.325	4.362	3.727	4.677	5.164	6.098
(0,1,0)	573.353	577.640	577.676	576.931	577.952	578.353	579.350
(0,2,0)	1160.443	1164.729	1164.762	1163.758	1164.834	1165.202	1166.246
(0,0,1)	1340.475	1344.772	1344.808	1344.167	1345.088	1345.599	1346.505
(1,0,0)	1342.732	1347.014	1347.050	1346.439	1347.370	1347.861	1348.776
(0,3,0)	1756.755	1761.076	1761.105	1760.285	1761.407	1761.784	1762.867
(1,1,0)	1912.375	1916.604	1916.652	1915.940	1916.943	1917.347	1918.327
(0,1,1)	1913.195	1917.453	1917.488	1916.748	1917.727	1918.146	1919.117
(0,4,0)	2349.097	2353.470	2353.498	2353.032	2354.198	2354.606	2355.726
(1,2,0)	2495.486	2499.725	2499.758	2498.785	2499.846	2500.212	2501.242
(0,2,1)	2497.411	2501.666	2501.697	2500.702	2501.750	2502.131	2503.151
(0,0,2)	2659.862	2664.125	2664.145	2663.551	2664.475	2664.977	2665.864
(1,0,1)	2659.935	2664.194	2664.208	2663.590	2664.508	2665.014	2665.901
(2,0,0)	2682.720	2686.971	2687.006	2686.390	2687.294	2687.804	2688.693
(0,5,0)	2940.900	2945.314	2945.342	2944.461	2945.673	2946.099	2947.258
(1,3,0)	3087.825	3092.094	3092.125	3091.320	3092.431	3092.802	3093.874
(0,3,1)	3089.521	3093.808	3093.836	3093.047	3094.143	3094.528	3095.590
(1,1,1)	3227.971	3232.190	3232.208	3231.480	3232.478	3232.883	3233.836
(0,1,2)	3228.025	3232.242	3232.253	3231.595	3232.589	3232.999	3233.955
(2,1,0)	3251.972	3256.187	3256.221	3255.494	3256.468	3256.891	3257.844
(0,6,0)	3528.681	3533.176	3533.202	3532.531	3533.787	3534.270	3535.465
(1,4,0)	3676.158	3680.468	3680.506	3680.058	3681.209	3681.614	3682.723
(0,4,1)	3677.300	3681.638	3681.669	3681.212	3682.346	3682.755	3683.855
(0,2,2)	3807.101	3811.315	3811.321	3810.389	3811.401	3811.807	3812.817
(1,2,1)	3807.262	3811.474	3811.532	3810.520	3811.580	3811.942	3812.949
(2,2,0)	3832.609	3836.822	3836.852	3835.888	3836.922	3837.304	3838.310
(1,0,2)	3955.225	3959.437	3959.471	3958.856	3959.737	3960.264	3961.129
(0,0,3)	3961.249	3965.462	3965.490	3964.879	3965.748	3966.284	3967.137
(2,0,1)	4001.954	4006.192	4006.214	4005.581	4006.441	4006.997	4007.849
(3,0,0)	4002.514	4006.716	4006.755	4006.173	4007.068	4007.575	4008.448
(0,7,0)	4102.959	4107.536	4107.563	4106.643	4107.944	4108.486	4109.719
(1,5,0)	4263.376	4267.695	4267.757	4266.911	4268.107	4268.532	4269.680
(0,5,1)	4264.619	4268.999	4269.030	4268.188	4269.344	4269.765	4270.904

[a]An F_2 state has $J = N - 1/2$; an F_1 state has $J = N + 1/2$.

Table 5: Calculated rovibronic term values (in cm^{-1}) for selected (v_1, v_2, v_3) states of $\tilde{X}^2B_1$ ^{121}SbHD.

$N_{K_aK_c}$	0_{00}	1_{01}		1_{11}		1_{10}	
(v_1, v_2, v_3)	$F_1{}^a$	$F_2{}^a$	$F_1{}^a$	F_2	F_1	F_2	F_1
(0,0,0)	0.000	4.350	5.005	7.098	8.084	7.617	9.093
(0,1,0)	697.766	702.101	702.766	704.813	705.905	705.349	706.921
(0,0,1)	1341.853	1346.132	1346.778	1348.943	1349.906	1349.436	1350.879
(0,2,0)	1411.406	1418.210	1416.330	1415.520	1419.245	1418.558	1420.205
(1,0,0)	1874.013	1878.365	1878.995	1880.958	1881.901	1881.511	1882.937
(0,1,1)	2038.005	2042.267	2042.922	2045.041	2046.110	2045.548	2047.088
(0,3,0)	2138.823	2145.391	2143.610	2142.588	2146.297	2145.423	2147.142
(1,1,0)	2565.408	2569.756	2570.389	2572.310	2573.367	2572.891	2574.417
(0,0,2)	2660.391	2664.606	2665.239	2667.485	2668.435	2667.960	2669.375
(0,2,1)	2748.396	2755.199	2753.239	2752.450	2756.227	2755.531	2757.147
(0,4,0)	2865.622	2872.510	2870.594	2869.746	2873.677	2872.932	2874.719
(1,0,1)	3215.013	3219.373	3219.947	3222.055	3223.021	3222.658	3224.053
(1,2,0)	3270.607	3277.302	3275.533	3274.776	3278.328	3277.736	3279.341
(0,1,2)	3354.233	3358.488	3359.097	3361.353	3362.444	3361.897	3363.409
(0,3,1)	3471.491	3478.062	3476.204	3475.222	3478.982	3478.104	3479.795
(0,5,0)	3576.835	3581.374	3582.024	3584.301	3585.756	3585.173	3587.016
(2,0,0)	3702.084	3706.585	3707.099	3709.067	3710.057	3709.802	3711.176
(1,1,1)	3906.584	3911.162	3911.598	3914.028	3915.252	3914.876	3916.369
(0,0,3)	3956.362	3960.444	3961.097	3963.359	3964.267	3963.748	3965.140
(1,3,0)	3988.483	3994.926	3993.282	3992.302	3995.821	3995.044	3996.729
(0,2,2)	4060.889	4065.167	4065.771	4068.048	4069.239	4068.644	4070.234
(0,4,1)	4193.778	4200.653	4198.660	4197.830	4201.817	4201.049	4202.810
(0,6,0)	4274.426	4281.612	4279.520	4278.579	4282.869	4282.129	4284.029
(2,1,0)	4388.109	4392.967	4393.246	4396.119	4397.465	4397.235	4398.709
(1,0,2)	4535.610	4539.873	4540.441	4542.576	4543.512	4543.129	4544.493
(1,2,1)	4610.771	4615.543	4615.866	4618.825	4620.259	4619.893	4621.464
(0,1,3)	4651.266	4657.932	4655.887	4655.120	4658.847	4658.121	4659.623
(1,4,0)	4705.247	4711.980	4710.211	4709.383	4713.122	4712.445	4714.205
(0,3,2)	4778.781	4782.889	4783.604	4785.717	4786.886	4786.179	4787.845
(0,5,1)	4900.791	4905.257	4905.891	4908.263	4909.715	4909.108	4910.923
(0,7,0)	4952.414	4956.957	4957.747	4960.167	4961.679	4961.100	4963.053
(2,0,1)	5048.841	5053.145	5053.700	5055.591	5056.490	5056.175	5057.514
(2,2,0)	5086.907	5092.000	5092.144	5096.985	5098.564	5098.366	5099.895

[a]An F_2 state has $J = N - 1/2$; an F_1 state has $J = N + 1/2$.

Table 6: Calculated rovibronic term values[a] (in cm^{-1}) for selected (v_1, v_2, v_3) states of $^{121}SbH_2$, $^{121}SbD_2$, and $^{121}SbHD$ in the $\tilde{A}^2A_1$ electronic state.

$N_{K_aK_c}$	0_{00}	1_{01}		1_{11}		1_{10}	
(v_1, v_2, v_3)	F_1[b]	F_2[b]	F_1[b]	F_2	F_1	F_2	F_1
				$^{121}SbH_2$			
(0,0,0)	19459.840[c]	6.108	6.258	20.860	12.665	21.627	13.281
(0,1,0)	696.519	702.603	702.770	720.219	709.652	721.034	710.251
(0,2,0)	1367.832	1373.922	1374.082	1395.167	1381.170	1396.041	1381.741
(1,0,0)	1630.498	1636.363	1636.528	1652.740	1643.327	1653.430	1643.851
(0,0,1)	1708.391	1714.194	1714.362	1730.736	1721.114	1731.387	1721.603
(0,3,0)	2020.780	2026.910	2027.023	2052.758	2033.869	2053.699	2034.399
(1,1,0)	2310.479	2316.309	2316.489	2336.172	2323.649	2336.911	2324.148
(0,1,1)	2378.590	2384.361	2384.541	2404.448	2391.499	2405.142	2391.924
(0,4,0)	2687.239	2693.442	2693.515	2723.753	2699.686	2724.801	2700.199
(1,2,0)	2970.521	2976.348	2976.503	3000.706	2983.589	3001.520	2984.057
(0,2,1)	3030.311	3036.097	3036.237	3060.636	3043.032	3061.402	3043.461
(2,0,0)	3094.183	3099.753	3099.937	3118.357	3106.940	3118.955	3107.351
(1,0,1)	3125.627	3131.159	3131.340	3149.915	3138.316	3150.493	3138.711
(0,0,2)	3325.434	3330.986	3331.173	3349.414	3338.169	3349.971	3338.558
(0,5,0)	3383.719	3389.933	3390.007	3427.061	3394.957	3428.198	3395.418
				$^{121}SbD_2$			
(0,0,0)	19505.590[c]	3.099	3.170	10.282	6.351	10.669	6.667
(0,1,0)	484.616	487.698	487.760	496.169	491.146	496.558	491.440
(0,2,0)	940.595	943.696	943.735	953.300	947.210	953.713	947.500
(1,0,0)	1194.848	1197.861	1197.934	1205.623	1201.271	1205.979	1201.551
(0,0,1)	1268.927	1271.915	1271.988	1279.732	1275.312	1280.076	1275.580
(0,3,0)	1418.411	1421.542	1421.576	1431.897	1425.054	1432.353	1425.359
(1,1,0)	1660.188	1663.184	1663.240	1672.486	1666.765	1672.842	1667.019
(0,1,1)	1726.602	1729.575	1729.630	1738.960	1733.113	1739.304	1733.355
(0,4,0)	1898.972	1902.104	1902.136	1913.938	1905.595	1914.415	1905.885
(1,2,0)	2116.250	2119.273	2119.308	2129.578	2122.868	2129.968	2123.127
(0,2,1)	2180.004	2183.010	2183.043	2193.311	2186.538	2193.688	2186.787
(2,0,0)	2319.462	2322.377	2322.452	2330.876	2325.926	2331.197	2326.166
(1,0,1)	2357.384	2360.276	2360.350	2368.848	2363.807	2369.163	2364.040
(0,5,0)	2377.643	2380.798	2380.824	2393.947	2384.168	2394.459	2384.455
(0,0,2)	2472.625	2475.510	2475.585	2484.083	2479.027	2484.385	2479.250
				$^{121}SbHD$			
(0,0,0)	19483.120[c]	15.715	4.101	15.715	9.498	16.161	9.736
(0,1,0)	602.697	620.374	606.374	620.374	612.487	620.840	612.697
(0,2,0)	1171.427	1191.656	1175.503	1191.656	1181.323	1192.146	1181.510
(0,0,1)	1231.040	1247.586	1234.996	1247.586	1240.666	1247.987	1240.805
(1,0,0)	1671.595	1688.225	1675.591	1688.225	1681.052	1688.621	1681.289
(0,3,0)	1732.881	1755.229	1736.966	1755.229	1742.665	1755.769	1742.853
(0,1,1)	1816.940	1835.875	1820.870	1835.875	1826.802	1836.291	1826.892
(1,1,0)	2244.000	2263.249	2247.973	2263.249	2253.624	2263.662	2253.842
(0,4,0)	2322.370	2346.833	2326.465	2346.833	2331.910	2347.442	2332.093
(0,0,2)	2358.673	2376.305	2362.461	2376.305	2368.398	2376.725	2368.414
(0,2,1)	2375.177	2396.820	2379.114	2396.820	2385.023	2397.249	2385.094
(1,2,0)	2791.507	2813.583	2795.463	2813.583	2800.971	2814.029	2801.174
(1,0,1)	2879.168	2896.948	2883.016	2896.948	2888.699	2897.306	2888.846
(0,5,0)	2916.760	2944.889	2920.828	2944.889	2925.732	2945.842	2925.899
(0,1,2)	2922.739	2942.840	2942.840	2932.517	2943.309	2932.502	2943.126

[a]Unless otherwise indicated the term values are relative to the $(v_1, v_2, v_3, N_{K_aK_c}, J) = (0, 0, 0, 0_{00}, 1/2)$ term value in the $\tilde{A}^2A_1$ electronic state of the molecule in question.

[b]An F_2 state has $J = N - 1/2$; an F_1 state has $J = N + 1/2$.

[c]Relative to the energy of the $(v_1, v_2, v_3, N_{K_aK_c}, J) = (0, 0, 0, 0_{00}, 1/2)$ level in the $\tilde{X}^2B_1$ electronic state of the molecule in question.

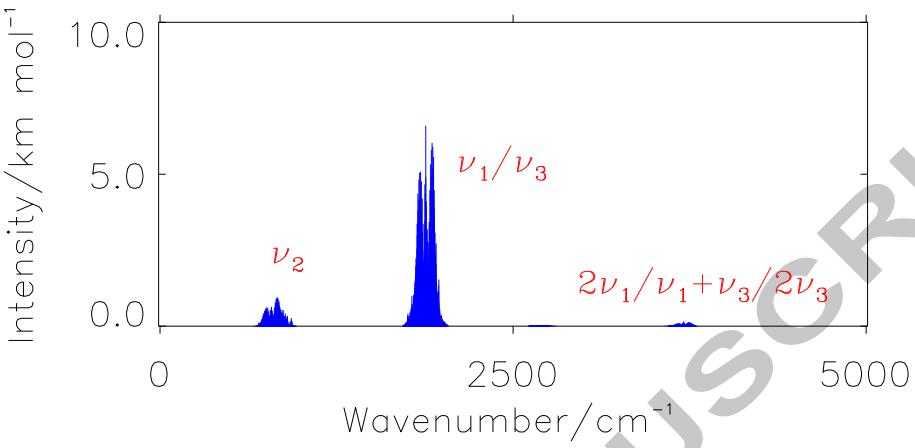

Figure 4: The infrared absorption spectrum of $\tilde{X}^2B_1$ $^{121}SbH_2$ and $^{123}SbH_2$ in natural abundance, simulated at a temperature of $T = 300$ K. States with $J \leq 19/2$ are taken into account.

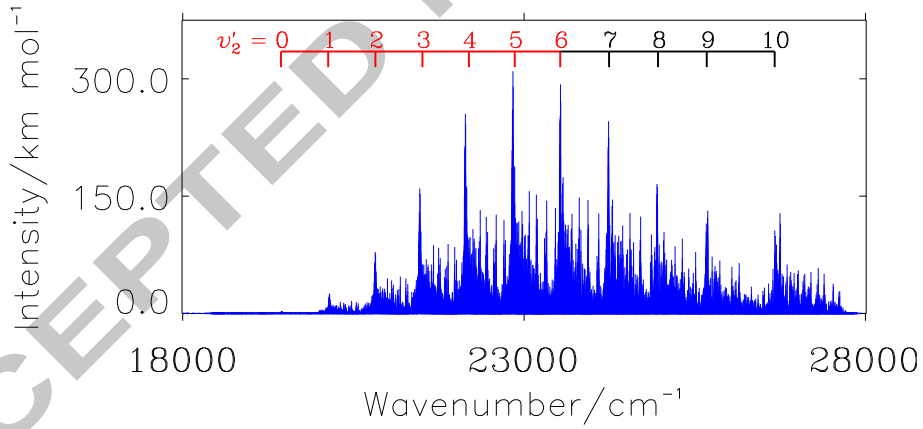

Figure 5: The $\tilde{A}^2A_1 \leftarrow \tilde{X}^2B_1$ electronic absorption spectrum of $^{121}SbH_2$ and $^{123}SbH_2$ in natural abundance, simulated at a temperature of $T = 300$ K. States with $J \leq 19/2$ are taken into account. The experimentally determined Q-branch-head positions [20] for the vibronic bands $\tilde{A}(0, v_2', 0) \leftarrow \tilde{X}(0, 0, 0)$ ($v_2' = 0, 1, \ldots, 6$; see Table 8) are indicated by the red part of the wavenumber comb, whereas the black part ($v_2' = 7, 8, 9, 10$) indicates the theoretically predicted positions of Q-branches that have not been experimentally observed.

Table 7: Stretching fundamental term values for $\widetilde{X}\,^2B_1$ SbH_2, SbD_2, and SbHD: Experimental values determined by Wang *et al.* [19] compared to values calculated in the present work.

Molecule	Environment	ν_1/cm^{-1}	ν_3/cm^{-1}
SbH_2	pure H_2	1869.7	1878
	Ne/H_2	1879.0	1883.9
	Ar/H_2	1863.7	1869.0
$^{121}SbH_2$	Calc.[a]	1876.0	1873.4
SbD_2	pure D_2	1341.9	1345.8
	Ne/D_2	1349.4	1352.0
	Ar/D_2	1337.6	1341.8
$^{121}SbD_2$	Calc.[b]	1342.7	1340.5
SbHD	Ar/HD	1339.6	1866.5
^{121}SbHD	Calc.[c]	1341.9	1874.0

[a]Values calculated in the present work (Table 3). [b]Values calculated in the present work (Table 4). [c]Values calculated in the present work (Table 5).

A spectrum attributed to the absorption spectrum of SbH_2 ($\tilde{A} \leftarrow \tilde{X}$) was obtained in Ref. [20] by flash photolysis of stibine (SbH_3). The positions of the Q-heads of the seven observed bands in the region from 420 nm to 520 nm are given in Table II of Ref. [20]. Our simulation of this region of the absorption spectrum [involving 200398(208869) transitions of $^{121}SbH_2(^{123}SbH_2)$] is given in Fig. 5; it is seen to be dominated by a progression of strong Q branches belonging to the vibronic bands $\tilde{A}(0, v_2', 0) \leftarrow \tilde{X}(0, 0, 0)$, $v_2' = 0$, 1, 2, ... For $v_2' \leq 6$, the corresponding Q-head positions have been experimentally observed [20]; the experimental wavenumbers are indicated by the red part of the wavenumber comb in the figure. We predict that the regular Q-branch progression continues for $v_2' = 7$, 8, 9. The Q branch predicted for $v_2' = 10$ is irregular in that it is stronger than expected from the intensity sequence of the Q branches with lower v_2' values. Also, the wavenumber spacing between the Q branches with $v_2' = 9$ and 10 is significantly larger than those between the lower-lying Q branches. Presumably, these irregularities are caused by the $\tilde{A}(0, 10, 0)$ state being close to the top of the barrier to linearity (see Fig. 3, the $\tilde{A}$-state bending level with $v_2' = 10$ is the highest one included in the figure). In Table 8, we compare the experimentally observed Q-head wavenumbers $\tilde{\nu}_{\rm obs}$ from Ref. [20] with the calculated positions $\tilde{\nu}_{\rm calc}$ obtained as the calculated term values of the $\tilde{A}(0, v_2', 0)$, $(N_{K_aK_c}, J) = (0_{00}, 1/2)$ level [$v_2' = 0$, 1, 2, ..., 6] of $^{121}SbH_2$ measured relative to the $\tilde{X}(0, 0, 0)$, $(N_{K_aK_c}, J) = (0_{00}, 1/2)$ level. It is seen that, as indicated also by Fig. 5, the calculated positions are in very good agreement with the observed values. The maximum relative deviation is 0.2%. In Table 8, we have also included the observed values of $\delta_{\rm obs} = \tilde{\nu}_{\rm obs} - 19438$ cm^{-1}. These values are approximately equal to the term values of the $\tilde{A}(0, v_2', 0)$, $(N_{K_aK_c}, J) = (0_{00}, 1/2)$ levels relative to the $\tilde{A}(0, 0, 0)$, $(N_{K_aK_c}, J) = (0_{00}, 1/2)$ level, and we compare them in the table to the corresponding calculated values $\delta_{\rm calc} = \tilde{\nu}_{\rm calc} - 19459.8$ cm^{-1} obtained from Table 6 (but augmented by the calculated term values for $v_2' = 6$, ..., 10 which are not included in Table 6). Obviously, the agreement with the experimentally derived values is very satisfactory, the relative deviation being only -3.5 cm^{-1}, or -0.5%, for $v_2' = 1$ and never larger in size than 2.5% for higher values of v_2'.

In Ref. [21] the emission spectrum of SbH_2 ($\tilde{A} \rightarrow \tilde{X}$) from 400 to 700 nm was recorded with a reported resolution of 12 Å. A portion of the spectrum from 480 to 530 nm was recorded with a reported resolution of 3 Å. These spectra are shown in Fig. 1 of Ref. [21] and we reproduce them in the top half

Table 8: Experimentally observed Q-head positions $\tilde{\nu}_{\rm obs}$ ($\rm cm^{-1}$) in the $\tilde{A}^2A_1 \leftarrow \tilde{X}^2B_1$ absorption spectrum of SbH_2 [20] compared to vibronic energy spacings $\tilde{\nu}_{\rm calc}$ ($\rm cm^{-1}$) of $^{121}SbH_2$.

$(v_2')^a$	$\tilde{\nu}_{\rm obs}$	$\tilde{\nu}_{\rm calc}{}^b$	O−C^c	$\Delta_{\%}{}^d$	$\delta_{\rm obs}{}^e$	$\delta_{\rm calc}{}^f$	O−C^g	$\Delta_{\%}{}^h$
0	19438	19459.8	−22	−0.1	0	0.0		
1	20131	20156.4	−25	−0.1	693	696.5	−3.5	−0.5
2	20822	20827.7	−6	0.0	1384	1367.8	16.2	1.2
3	21511	21480.6	30	0.1	2073	2020.7	52.3	2.5
4	22191	22147.1	44	0.2	2753	2687.2	65.8	2.4
5	22863	22843.6	19	0.1	3425	3383.7	41.3	1.2
6	23529	23539.8	−11	0.0	4091	4080.0	11.0	0.3
7		24244.3				4784.5		
8		24961.5				5501.7		
9		25675.1				6215.3		
10		26669.9				7210.1		

[a] v_2' defines the upper state of the vibronic band $\tilde{A}(0, v_2', 0) \leftarrow \tilde{X}(0, 0, 0)$.
[b] Calculated term value (in $\rm cm^{-1}$) of the $\tilde{A}(0, v_2', 0)$, $(N_{K_aK_c}, J) = (0_{00}, 1/2)$ level of $^{121}SbH_2$ [relative to the $\tilde{X}(0, 0, 0)$, $(N_{K_aK_c}, J) = (0_{00}, 1/2)$ level].
[c] $\tilde{\nu}_{\rm obs} - \tilde{\nu}_{\rm calc}$, in $\rm cm^{-1}$.
[d] $100 \times (\tilde{\nu}_{\rm obs} - \tilde{\nu}_{\rm calc})/\tilde{\nu}_{\rm obs}$.
[e] $\delta_{\rm obs} = \tilde{\nu}_{\rm obs} - 19438$ $\rm cm^{-1}$, in $\rm cm^{-1}$.
[f] $\delta_{\rm calc} = \tilde{\nu}_{\rm calc} - 19459.8$ $\rm cm^{-1}$, in $\rm cm^{-1}$.
[g] $\delta_{\rm obs} - \delta_{\rm calc}$, in $\rm cm^{-1}$.
[h] $100 \times (\delta_{\rm obs} - \delta_{\rm calc})/\delta_{\rm obs}$.

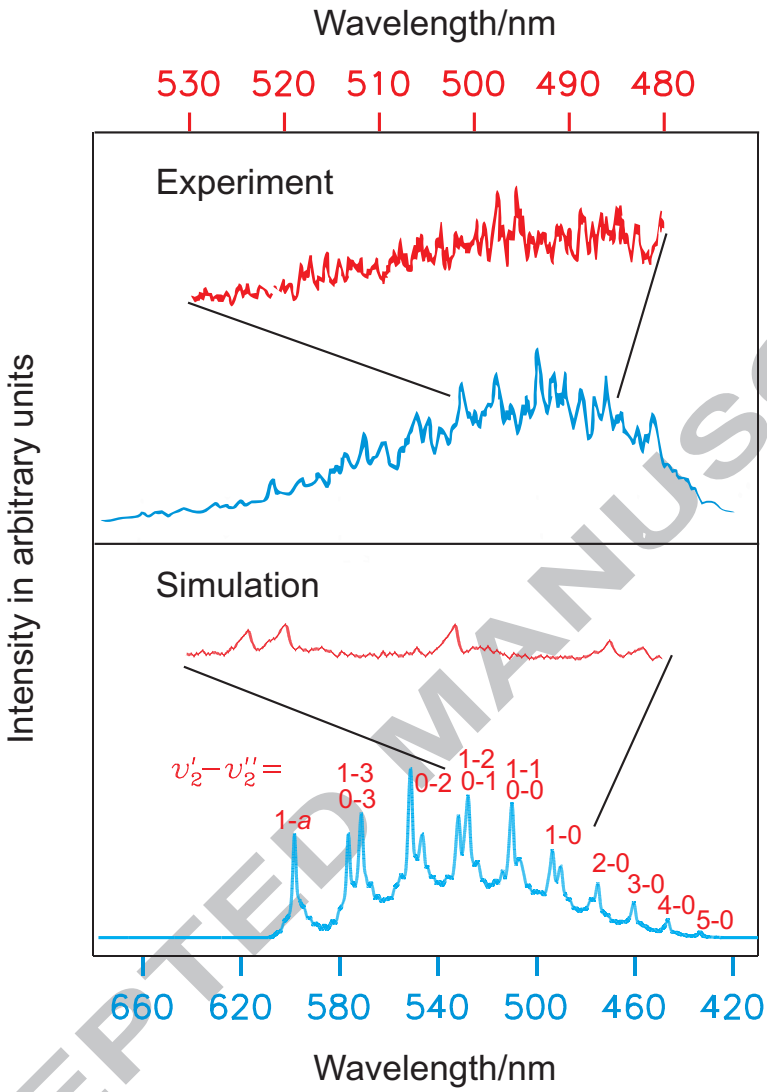

Figure 6: The $\tilde{A}^2A_1 \rightarrow \tilde{X}^2B_1$ emission spectrum of $^{121}SbH_2$ and $^{123}SbH_2$ in natural abundance, simulated at a temperature of $T = 1200$ K and including transitions between states with $J \leq 49/2$ (see text). The experimental curves are reproduced from Fig. 1 of Ref. [21] by kind permission from Elsevier. The blue(red) curves represent spectra with a reported resolution of 12(3) Å (see text) and are consistent with the blue(red) abscissa tick marks at the bottom(top) of the diagram. We have given tentative assignments of the stronger features; they are generally Q branches belonging to bands of the type $\tilde{A}(0, \upsilon_2', 0) \rightarrow \tilde{X}(0, \upsilon_2'', 0)$. The feature labeled $1 - a$ contains Q branch transitions of the vibronic band $\tilde{A}(0, 1, 0) \rightarrow \tilde{X}(1, 2, 0)$.

of Fig. 6 here.[2] We have simulated these spectra, using as starting points line lists calculated with RENNER basis set (c) and $J \leq 49/2$ for $^{121}SbH_2$ and $^{123}SbH_2$ in natural abundance. The basis set was reduced in size relative to basis set (a) to save computer resources, in particular CPU time, since a reduction of the accuracy is acceptable in the calculation of these low-resolution spectra. The spectra of Ref. [21] are given in terms of wavelength λ and a transition calculated by RENNER with the wavenumber $\tilde{\nu}$ is found at the wavelength $\lambda = 1/\tilde{\nu}$. The calculations produced 62213 transitions for each of the two molecules $^{121}SbH_2$ and $^{123}SbH_2$. We simulate the low-resolution spectra by 'binning' the wavelength-dependent line list into bins of width 0.01 nm (so that the transitions in each bin are approximated by a single transition located at the center wavelength of the bin and having an intensity equal to the sum of the intensities of all transitions in the bin) and convolving, by numerical integration, the binned spectrum with Gaussians having full widths at half height of 12 and 3 Å, respectively.

To simulate the emission spectrum it is necessary to model the population distribution in the SbH_2 rovibronic energy levels at the onset of the emission. We do this as described in Ref. [40]: By analyzing the eigenvector coefficients from our calculation we determine that some levels are predominantly $\tilde{A}^2A_1$ state levels and the rest are predominantly $\tilde{X}^2B_1$ state levels. We model the initial population distribution as a Boltzmann distribution in the rovibronic levels that are predominantly $\tilde{A}^2A_1$ state levels, and we assume that the other rovibronic levels are unpopulated. By trial and error, we estimate the Boltzmann distribution temperature in the $\tilde{A}^2A_1$ state levels to be 1200 K since lower temperatures produce extremely weak and much too narrow simulated spectra. Our simulation of the emission spectrum is included in Fig. 6. In this figure we have attempted the difficult task of assigning the strong features of the simulated spectrum. Because of the high temperature (1200 K) necessary to obtain a simulated spectrum of a width comparable to that of the experimental one, the simulated spectrum has a plethora of P, Q, and R lines everywhere. At or near the positions of the strong features we have identified Q branches of closely spaced transitions which we assume deliver the major contribution to the strong features. Most

[2]Reprinted from Fig. 1 of Chemical Physics Letters, Vol. 128, Tuqiang Ni, Shuqin Yu, Xingxiao Ma, and Fanao Kong, The UV laser photolysis of stibine, pp. 270–273, Copyright 1986, with kind permission from Elsevier.

of these Q branches belong to bands of the type $\tilde{A}(0, v_2', 0) \rightarrow \tilde{X}(0, v_2'', 0)$. The one exception is the feature labeled $1-a$ in Fig. 6; it contains Q branch transitions of the vibronic band $\tilde{A}(0, 1, 0) \rightarrow \tilde{X}(1, 2, 0)$.

The comparison of our simulation with the experimental spectrum of Ref. [21] is given in Fig. 6, and it is clearly not convincing. The reasons for this form the major part of the discussion in Section 6.

5. LOCAL MODE VIBRATIONS AND ROVIBRONIC ENERGY CLUSTERS

The term values of Tables 3 and 4 show that $\tilde{X}^2B_1$ SbH_2 and SbD_2 are local mode molecules (see Refs. [41, 42] and references therein). Stretching states $(v_1, 0, v_3)$ with a common value of $v_1 + v_3 = N$ are close in energy and form characteristic patterns. For N even, there are $N/2$ energy pairs with the pair consisting of the states $(N, 0, 0)$ and $(0, 0, N)$ being at lowest energy followed, in order of increasing energy, by pairs formed by the states $[(N-1, 0, 1), (1, 0, N-1)]$, $[(N-2, 0, 2), (2, 0, N-2)]$, ... The 'lonely' state $(N/2, 0, N/2)$ is at the highest energy in the manifold. The splitting between the energies of the pair members is smallest for the $[(N, 0, 0), (0, 0, N)]$ pair at lowest energy and largest for the $[(N/2-1, 0, N/2+1), (N/2+1, 0, N/2-1)]$ pair at highest pair energy. For N odd, there are $(N + 1)/2$ energy pairs, again with $[(N, 0, 0), (0, 0, N)]$ being at lowest energy and having the smallest splitting while the pair $[((N+1)/2, 0, (N-1)/2), ((N-1)/2, 0, (N+1)/2)]$ is at largest energy and has the largest splitting. The energy patterns are explained in terms of the Harmonically-Coupled-Anharmonic-Oscillator (HCAO) model [43, 44, 45] (see also Refs. [41, 42, 46, 47, 48]). In reality, the characteristic patterns are sometimes 'spoiled' by interactions with nearby (v_1, v_2, v_3) states having $v_2 > 0$; these states are not accounted for by the HCAO model.

The vibrational energy level clusters caused by local-mode effects are accompanied by rovibronic energy clusters at high rotational excitation [41, 42, 49], analogous to the ones formed in the $\tilde{X}^2B_1$ and $\tilde{A}^2A_1$ electronic states of the PH_2 radical [50]. Figures 7 and 8 show examples of this; they are term value diagrams for the vibrational ground state, and the combined ν_1/ν_3 states, respectively, of $\tilde{X}^2B_1$ $^{121}SbH_2$. The term values are calculated with RENNER basis set (d). In both diagrams, we recognize the formation of four-fold energy clusters, the states in each cluster being of symmetry $A_1 \oplus A_2 \oplus B_1 \oplus B_2$ [51] in the molecular symmetry group [38, 52] $\boldsymbol{C}_{2v}$(M). The

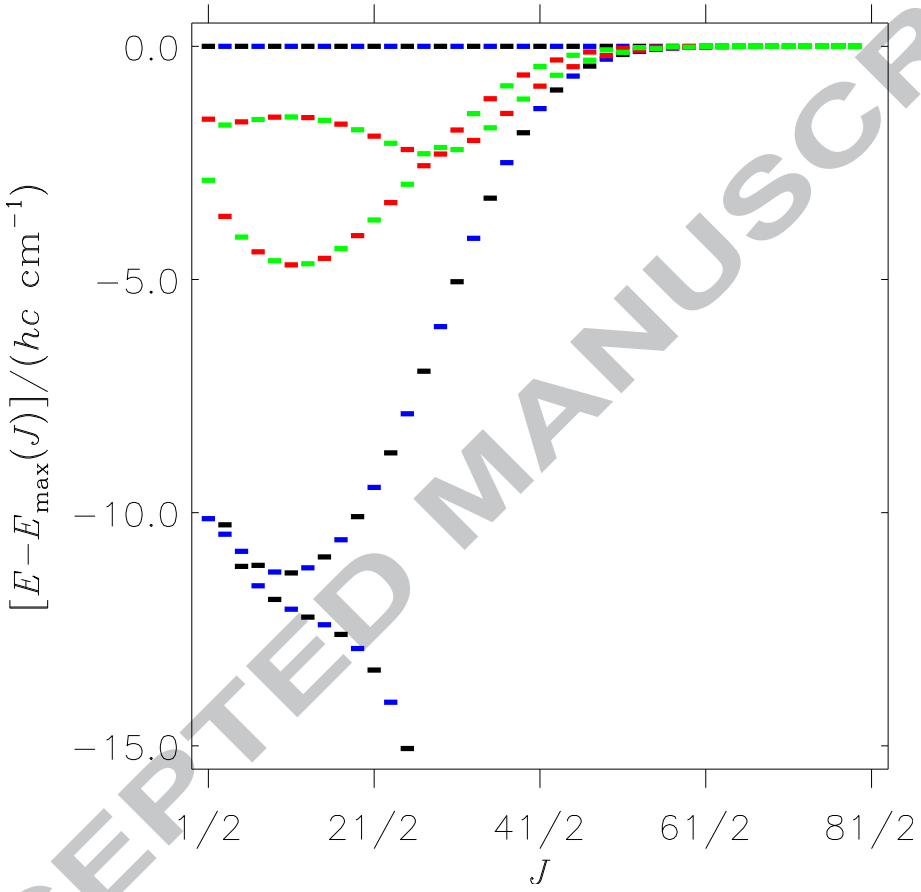

Figure 7: Rotational term level diagram for the vibrational ground state of $\tilde{X}^2B_1$ ^{121}SbH_2. The energies are plotted relative to the highest energy in each J manifold. The term values are colour-coded according to the symmetry of the state in the molecular symmetry group [38, 52] $\boldsymbol{C}_{2\mathrm{v}}$(M): A_1 (red), A_2 (black), B_1 (blue), and B_2 (green).

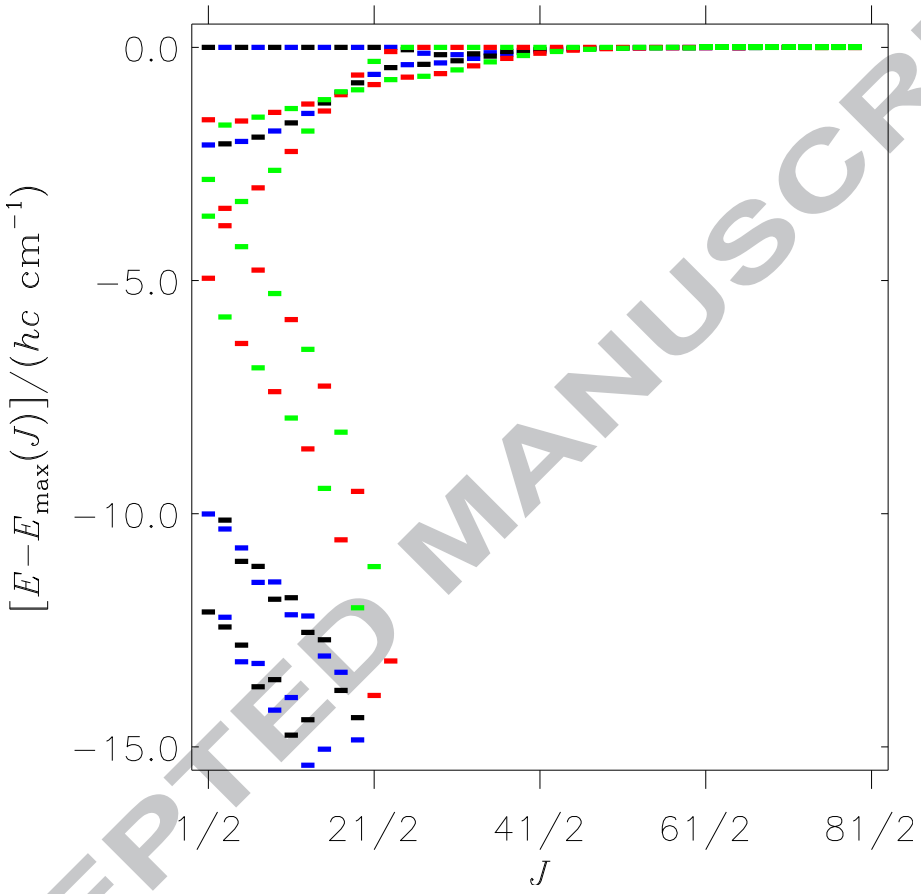

Figure 8: Rotational term level diagram for the ν_1 and ν_3 vibrational states of $\tilde{X}^2B_1$ ^{121}SbH_2. The energies are plotted relative to the highest energy in each (combined ν_1 and ν_3) J manifold. The term values are colour-coded according to the symmetry of the state in the molecular symmetry group [38, 52] $\boldsymbol{C}_{2\mathrm{v}}$(M): A_1 (red), A_2 (black), B_1 (blue), and B_2 (green).

energy clusters in Fig. 7 are of Type I [53]; they involve only one vibrational state, the vibrational ground state of $\tilde{X}^2B_1$ SbH_2. The energy clusters in Fig. 8 are formed by the merging (with increasing J) of two energy doublets, one doublet belonging to the ν_1 vibrational state and the other one to the ν_3 vibrational state. Such clusters are of Type II [53].

The appearance of Figs. 7 and 8 differs from that of the analogous diagrams shown for PH_2 in Ref. [50] since in Figs. 7 and 8, we plot the term values against J whereas for PH_2 [50], we plotted them against N. In spite of the differences in the appearance of the diagrams, the energy level pattern for SbH_2 is completely analogous to that of PH_2.

6. DISCUSSION AND COMPARISON WITH EXPERIMENT

The main aim of this work is to make *ab initio* simulations of the absorption and emission spectra of SbH_2 in order to corroborate the spectroscopic identifications made in Refs. [19, 20, 21]. In Table 7, we summarize the matrix isolation infrared spectroscopic results of Ref. [19], in which laser ablated Sb atoms were reacted with hydrogen during condensation, and compare them to our predicted fundamental wavenumbers. The comparison supports the assignment to SbH_2, SbD_2, and SbHD, respectively, but it predicts that for SbH_2 and SbD_2, $E(\nu_1) > E(\nu_3)$ whereas the assignment of Ref. [19] assumes the more usual situation of $E(\nu_3) > E(\nu_1)$. The experimental assignment is an assumption since the matrix isolation spectra of Ref. [19] do not provide resolved rotational structure from which the two vibrational bands can be unambiguously identified (strong transitions in the ν_1 band have $\Delta K_a = \pm 1$ whereas in the ν_3 band they have $\Delta K_a = 0$). A high resolution spectroscopic gas phase study would be of interest to determine the true experimental assignment. We also found a favorable comparison between the experimentally observed Q-band-head positions in the $\tilde{A} \leftarrow \tilde{X}$ gas phase electronic absorption spectrum of SbH_2 [20] and our calculated values for the corresponding vibronic energy spacings in $^{121}SbH_2$ (Table 8). This shows that the observed spectrum of Ref. [20] can be unequivocably assigned to SbH_2. In contrast to these two favorable comparisons, the $\tilde{A} \rightarrow \tilde{X}$ emission spectrum of SbH_2, experimentally observed by Ni *et al.* [21], and our simulation (Fig. 6) do not compare favorably. However, there are considerable problems with this spectrum, both experimentally and theoretically, and the rest of this section is devoted to discussing this.

In the experiment by Ni *et al.* [21], SbH_2 molecules were produced by ArF laser photolysis of SbH_3. If Ni *et al.* [21] are describing the experiment precisely, they scanned their emission monochromator from a start at 403 nm to an end of 700 nm. At the same time, Sb was depositing on the front window of the photolysis cell, and so one would expect [54] the emission spectrum to have unrealistically low intensity at the high-wavelength end, since the transmission of the ArF laser beam decreases throughout the scan of the emission spectrum. This seems to be exactly what our calculations suggest (Fig. 6). The onset at the low-wavelength end is about the same for the experimental and simulated spectra, but the experimental spectrum tails off more rapidly than calculated. Also, the lack of similarity between the 3-Å-resolution spectrum and the 12-Å-resolution spectrum is remarkable. The 3-Å-resolution spectrum spans a region that includes a strong peak at the high-wavelength end of the 12-Å-resolution spectrum. We do not see this peak at all in the 3-Å-resolution spectrum and this indicates that the noise level is substantial in the experimental spectra.

On the theoretical side, our description of the initial population distribution in the $\tilde{A}$-state levels is simplistic. For lack of knowledge about the actual population distribution resulting from the ArF laser photolysis of SbH_3, we take the SbH_2 molecules to be Boltzmann distributed over the $\tilde{A}$-state levels at a temperature of 1200 K. This temperature is very high but as pointed out above, tests with lower temperatures produced simulations covering a much too narrow wavelength interval. Also, the high temperature is in keeping with the statement of Ni *et al.* [21] that "the vibrational bands of the spectrum are extremely complicated and difficult to assign, partly because SbH_2 $\tilde{A}^2A_1$ state has a highly vibrationally excited population." It seems likely that the ArF laser photolysis of SbH_3 could lead to a non-Boltzmann population distribution of the SbH_2 molecules produced which we cannot correctly simulate. Another, less important theoretical problem is that even in the case that the assumption of a Boltzmann population distribution is satisfactory, levels with $J > 49/2$, which we cannot consider because of computer limitations, may be populated at $T = 1200$ K. In view of these difficulties, there is nothing in the present work that contradicts the assignment of SbH_2 as the carrier of the experimental spectrum which, it would seem, is of somewhat questionable quality.

We hope that the results of the present work will encourage and assist further experimental investigations of the spectra of SbH_2 and its isotopologues.

Acknowledgments

We thank Professor Dennis J. Clouthier for helpful correspondence, and we are grateful to the anonymous reviewer of the initial version of this work for pointing out that we were using an incorrect A_{SO} value, and for a generally scathing criticism of our work motivating us to scrutinize it, thus finding an additional mistake. The correction of these two mistakes improved greatly the agreement with the experimental results of Refs. [19, 20]. B. O. gratefully acknowledges the financial support of the Ministry of Education, Science and Technological Development of the Republic of Serbia (Contract No. 172001). The work of P. J. is supported in part by the Deutsche Forschungsgemeinschaft and the Fonds der Chemischen Industrie. P. R. B. is grateful to Massey University for hospitality.

[1] K. P. Huber and G. Herzberg, *"Molecular Spectra and Molecular Structure,"* Van Nostrand Reinhold Company Inc., New York, 1979.

[2] H. G. Hedderich and P. F. Bernath, J. Mol. Spectrosc. 158 (1993) 170-176.

[3] S. Aldridge and A. J. Downs, Chem. Rev. 101 (2001) 3305-3365.

[4] P. Schwerdtfeger, G. A. Heath, M. Dolg and M. A. Bennett, J. Am. Chem. Soc. 114 (1992), 7518-7527.

[5] W. Liu, Ch. v. Wüllen, F. Wang and L. Li, J. Chem. Phys. 116 (2002) 3626-3634.

[6] S. Knecht, H. J. Aa. Jensen and T. Fleig, J. Chem. Phys. 132 (2010) 014108.

[7] L. K. Sørensen, J. Olsen and T. Fleig, J. Chem. Phys. 134 (2011) 214102.

[8] W. Jerzembeck, H. Bürger, L. Constantin, L. Margulés, J. Demaison, J. Breidung and W. Thiel, Angew. Chem. Int. Ed. 41 (2002) 2550-2552.

[9] P. Schwerdtfeger, L. J. Laakkonen, P. Pyykkö, J. Chem. Phys. 96 (1992) 6807-6819.

[10] P. Jensen, T. E. Odaka, W. P. Kraemer, T. Hirano, and P. R. Bunker, Spectrochimica Acta part A 58 (2002) 763-794.

[11] S. N. Yurchenko, W. Thiel, P. Jensen and P. R. Bunker, J. Mol. Spectrosc. 239 (2006) 160-173.

[12] A. B. Alekseyev, R. J. Buenker and H. P. Liebermann, J. Chem. Phys. 135 (2011) 244303/1-8.

[13] P. Jensen, J. Mol. Spectrosc. 128 (1988) 478-501.

[14] G. Duxbury and A. Alijah, Abstract WI03, 69th International Symposium on Molecular Spectroscopy, Champaign-Urbana, Illinois, U.S.A., 2014.

[15] R. A. Grimminger and D. J. Clouthier, J. Chem. Phys. 137 (2012) 224307/1-12.

[16] P. Jensen, M. Brumm, W. P. Kraemer, and P. R. Bunker, J. Mol. Spectrosc. 171 (1995) 31-57.

[17] M. Kolbuszewski, P. R. Bunker, W. P. Kraemer, G. Osmann, and P. Jensen, Mol. Phys. 88 (1996) 105-124.

[18] G. Osmann, P. R. Bunker, P. Jensen, and W. P. Kraemer, Chem. Phys. 225 (1997) 33-54.

[19] X. Wang, P. F. Souter and L. Andrews, J. Phys. Chem. A. 107 (2003) 4244-4249.

[20] N. Basco and K. K. Lee, Spectroscopy Letters 1 (1968) 13-15.

[21] T. Ni, S. Yu, X. Ma and F. Kong, Chem. Phys. Lett. 128 (1986) 270-273.

[22] L.-A. M. Smith-Freeman, Ph.D. dissertation, Department of Chemistry, University of Southern California, Los Angeles, U. S. A., 2009.

[23] H.-J. Werner, P. J. Knowles, J. Chem. Phys. 82 (1985) 5053-5063.

[24] P. J. Knowles, H.-J. Werner, Chem. Phys. Lett. 115 (1985) 259-267.

[25] H.-J. Werner, P. J. Knowles, J. Chem. Phys. 89 (1988) 5803-5814.

[26] P. J. Knowles, H.-J. Werner, Chem. Phys. Lett. 145 (1988) 514-522.

[27] P. J. Knowles, H.-J. Werner, Theor. Chim. Acta 84 (1992) 95-103.

[28] S. R. Langhoff, E. R. Davidson, Int. J. Quant. Chem. 8 (1974) 61-72.

[29] Segmented Gaussian Basis Set, Quantum chemistry group, Sapporo, Japan. See http://setani.sci.hokudai.ac.jp/sapporo/Welcome.do

[30] A. Canal Neto, F.E. Jorge, Chem. Phys. Lett. 582 (2013) 158-162.

[31] M. Reiher and A. Wolf, J. Chem. Phys. 121 (2004) 2037-2047.

[32] M. Reiher and A. Wolf, J. Chem. Phys. 121 (2004) 10945-10956.

[33] A. Wolf, M. Reiher, and B. A. Hess, J. Chem. Phys. 117 (2002) 9215-9226.

[34] H.-J. Werner, P. J. Knowles, G. Knizia, F. R. Manby, M. Schütz, P. Celani, T. Korona, R. Lindh, A. Mitrushenkov, G. Rauhut, K. R. Shamasundar, T. B. Adler, R. D. Amos, A. Bernhardsson, A. Berning, D. L. Cooper, M. J. O. Deegan, A. J. Dobbyn, F. Eckert, E. Goll, C. Hampel, A. Hesselmann, G. Hetzer, T. Hrenar, G. Jansen, C. Köppl, Y. Liu, A. W. Lloyd, R. A. Mata, A. J. May, S. J. McNicholas, W. Meyer, M. E. Mura, A. Nicklass, D. P. O'Neill, P. Palmieri, K. Pflüger, R. Pitzer, M. Reiher, T. Shiozaki, H. Stoll, A. J. Stone, R. Tarroni, T. Thorsteinsson, M. Wang, and A. Wolf, MOLPRO, version 2010.1, a package of *ab initio* programs. See http://www.molpro.net.

[35] K. A. Peterson, J. Chem. Phys. 119 (2003) 11099/1-xx.

[36] T. H. Dunning, Jr., J. Chem. Phys. 90 (1989) 1007-.

[37] E. Moore, Atomic Energy levels, National Bureau of Standards, Circular 467, Volume 3, Washington (1958).

[38] P. R. Bunker and P. Jensen, Molecular Symmetry and Spectroscopy, NRC Research Press, Ottawa, 1998.

[39] P. Jensen, J. Mol. Spectrosc. 132 (1988) 429-457.

[40] G. Osmann, P. R Bunker, P. Jensen, R. J. Buenker, J.-p. Gu, and G. Hirsch, J. Mol. Spectrosc. 197 (1999) 262-274.

[41] P. Jensen, Mol. Phys. 98 (2000) 1253-1285.

[42] P. Jensen, WIREs Comput. Mol. Sci. 2 (2012) 494-512.

[43] M. S. Child and R. T. Lawton, Faraday Discuss. Chem. Soc. 71 (1981) 273-285.

[44] O. S. Mortensen, B. R. Henry, and M. A. Mohammadi, J. Chem. Phys. 75 (1981) 4800-4808.

[45] M. S. Child and L. Halonen, Adv. Chem. Phys. 57 (1984) 1-58.

[46] L. Halonen, Adv. Chem. Phys. 104 (1998) 41-179.

[47] O. N. Ulenikov and S. N. Yurchenko, Russian Physics Journal 42 (1999) 458-461.

[48] L. Halonen, in Computational Molecular Spectroscopy, Eds. P. Jensen and P. R. Bunker, Wiley, Chichester, 2000, 325-364.

[49] P. Jensen, G. Osmann, and I. N. Kozin, in Advanced Series in Physical Chemistry: Vibration-Rotational Spectroscopy and Molecular Dynamics, Ed. D. Papoušek, vol. 9, World Scientific Publishing Company, Singapore, 1997, 298-351.

[50] S. N. Yurchenko, W. Thiel, P. Jensen, and P. R. Bunker, J. Mol. Spectrosc. 239 (2006) 160-173.

[51] P. Jensen and P. R. Bunker, J. Mol. Spectrosc. 164 (1994) 315-317.

[52] P. R. Bunker and P. Jensen, Fundamentals of Molecular Symmetry, IOP Publishing, Bristol, 2004.

[53] I. N. Kozin and P. Jensen, J. Mol. Spectrosc. 161 (1993) 186-207.

[54] D. J. Clouthier, private communication.

Title of manuscript: An *ab initio* study of SbH_2 and BiH_2: The Renner Effect, Spin-Orbit Coupling, Local Mode Vibrations and Rovibronic Energy Level Clustering in SbH_2

Corresponding Author: Prof. Per Jensen
Authors: Bojana Ostojic, Dr.; Peter A Schwerdtfeger, Prof.; Philip R Bunker, Dr.

Highlights

- For SbH_2 and BiH_2 we calculate *ab initio* the bending potential curves for the six lowest electronic states, and the spin-orbit coupling constant.
- For the two lowest, Renner-degenerate electronic states of SbH_2 we compute fully-dimensional potential energy surfaces.
- We simulate the IR and visible spectra of SbH_2 involving the two lowest electronic states, taking into account the strong spin-orbit coupling.
- The SbH_2 results are compared to available experimental data; excellent agreement is obtained with the results of matrix isolation infrared spectroscopic studies and with gas phase electronic spectroscopic studies in absorption.
- For SbH_2 we study local mode vibrations and rovibronic energy level clusters.
- First *ab initio* study of SbH_2 at spectroscopic precision.

*Graphical Abstract